Astronomy & Astrophysics manuscript no. LFI˙Programme˙Paper˙M1˙23jun09
June 24, 2009

Planck Pre-launch Status: the Planck-LFI Programme

N. Mandolesi[1], M. Bersanelli[2], R.C. Butler[1], E. Artal[7], C. Baccigalupi[8,35,6], A. Balbi[5], A.J. Banday[9,39], R.B. Barreiro[17], M. Bartelmann[9], K. Bennett[26], P. Bhandari[10], A. Bonaldi[3], J. Borril[38], M. Bremer[26], C. Burigana[1], R.C. Bowman[10], P. Cabella[5,45], C. Cantalupo[38], B. Cappellini[2], T. Courvoisier[11], G. Crone[12], F. Cuttaia[1], L. Danese[8], O. D'Arcangelo[13], R. Davies[14], R. Davis[14], L. De Angelis[15], G. de Gasperis[5], A. De Rosa[1], G. De Troia[5], G. De Zotti[3], J. Dick[8], C. Dickinson[14], J. M. Diego[17], S. Donzelli[22], U. Dörl[9], X. Dupac[40], T.A. Enßlin[9], H. K. Eriksen[22], M.C. Falvella[15], F. Finelli[1,34], M. Frailis[6], E. Franceschi[1], T. Gaier[10], S. Galeotta[6], F. Gasparo[6], G. Giardino[26], F. Gomez[18], J. Gonzalez-Nuevo[8], K.M. Górski[10,41], A. Gregorio[16], A. Gruppuso[1], F. Hansen[22], R. Hell[9], D. Herranz[17], J.M. Herreros[18], S. Hildebrandt[18], W. Hovest[9], R. Hoyland[18], K. Huffenberger[43], M. Janssen[10], T. Jaffe[9], E. Keihänen[19], R. Keskitalo[19,33], T. Kisner[38], H. Kurki-Suonio[19,33], A. Lähteenmäki[20], C.R. Lawrence[10], S. M. Leach[8,35], J. P. Leahy[14], R. Leonardi[21], S. Levin[10], P.B. Lilje[22], M. López-Caniego[42], S.R. Lowe[14], P.M. Lubin[21], D. Maino[2], M. Malaspina[1], M. Maris[6], J. Marti-Canales[12], E. Martinez-Gonzalez[17], S. Matarrese[4], F. Matthai[9], P. Meinhold[21], A. Melchiorri[45], L. Mendes[23], A. Mennella[2], G. Morgante[1], G. Morigi[1], N. Morisset[11], A. Moss[29], A. Nash[10], P. Natoli[5,36], R. Nesti[24], C. Paine[10], B. Partridge[25], F. Pasian[6], T. Passvogel[12], D. Pearson[10], L. Pérez-Cuevas[26], F. Perrotta[8,6], G. Polenta[44,45], L.A. Popa[27], T. Poutanen[33,19,20], G. Prezeau[10], M. Prina[10], J.P. Rachen[9], R. Rebolo[18], M. Reinecke[9], S. Ricciardi[37,38], T. Riller[9], G. Rocha[10], N. Roddis[14], R. Rohlfs[11], J.A. Rubiño-Martin[18], M. Sandri[1], D. Scott[29], M. Seiffert[10], J. Silk[30], A. Simonetto[13], G.F. Smoot[28,31], C. Sozzi[13], J. Sternberg[26], F. Stivoli[38], L. Stringhetti[1], J. Tauber[26], L. Terenzi[1], M. Tomasi[2], J. Tuovinen[32], M. Türler[11], L. Valenziano[1], J. Varis[32], P. Vielva[17], F. Villa[1], N. Vittorio[5,36], L. Wade[10], S. White[9], A. Wilkinson[14], A. Zacchei[6], A. Zonca[2]

(Affiliations can be found after the references)

Preprint online version: June 24, 2009

Abstract

This paper provides an overview of the Low Frequency Instrument (LFI) programme within the ESA Planck mission. The LFI instrument has been developed to produce high precision maps of the microwave sky at frequencies in the 27-77 GHz range, below the peak frequency of the Cosmic Microwave Background (CMB) radiation spectrum. The scientific goals are described, ranging from fundamental cosmology to Galactic and extragalactic astrophysics. The instrument design and development are outlined, together with the model philosophy and testing strategy. The instrument is presented in the context of the Planck mission. The LFI approach to on-ground and in-flight calibration is described. We also provide a description of the LFI ground segment. We present results of a number of tests that demonstrate the capability of the LFI Data Processing Centre (DPC) to properly reduce and analyse LFI flight data, from telemetry information to sky maps and other scientific products. The organization of the LFI Consortium is briefly presented as well as the role of the Core Team. All tests carried out on the LFI flight model show the excellent performance of the instrument and its various sub-units. The data analysis pipeline has been tested and its main functionalities proven. After the commissioning, calibration, performance, and verification phases are completed during the first three months after launch, Planck will begin its operational life, which LFI is fully ready to support.

Key words. (Cosmology): Cosmic Microwave Background – Galactic and extragalactic astrophysics – Space vehicles – Calibration – Data analysis

1. Introduction

In 1992 the Cosmic Background Explorer (COBE) team announced the discovery of intrinsic temperature fluctuations in the cosmic microwave background radiation (CMB; see appendix A for a list of the acronyms appearing in this paper) on angular scales larger than 7° and at a level of a few tens of μK Smoot et al. (1992). One year later two spaceborne CMB experiments were proposed to the European Space Agency (ESA) in the framework of the Horizon 2000 Scientific Programme: the Cosmic Background Radiation Anisotropy Satellite (COBRAS; Mandolesi et al. (1994)), an array of receivers based on High Electron Mobility Transistor (HEMT) amplifiers; and the SAtellite for Measurement of Background Anisotropies (SAMBA), an array of detectors based on bolometers (Tauber et al. 1994). The two proposals were accepted for assessment study with the recommendation to merge. In 1996 ESA selected a combined mission called COBRAS/SAMBA, subsequently renamed Planck, as the third Horizon 2000 Medium-Sized Mission. Today Planck forms part of "Horizon 2000" ESA Programme.

The address to which the proofs have to be sent is:
Nazzareno Mandolesi
INAF-IASF Bologna, Via Gobetti 101, I-40129, Bologna, Italy
fax: +39-051-6398681
e-mail: mandolesi@iasfbo.inaf.it

The Planck CMB anisotropy probe[1], the first European and third generation mission after COBE and WMAP (Wilkinson Microwave Anisotropy Probe), represents the state-of-the-art precision cosmology today (Tauber et al. 2009; Bersanelli et al. 2009; Lamarre et al. 2009). The Planck payload (telescope instrument and cooling chain) is a single, highly integrated spaceborne CMB experiment. Planck is equipped with a 1.5m effective aperture telescope with two actively-cooled instruments which will scan the sky in nine frequency channels from 30 GHz to 857 GHz: the Low Frequency Instrument (LFI) operating at 20K with pseudo-correlation radiometers, and the High Frequency Instrument (HFI) with bolometers operating at 100mK. Each instrument has a specific role in the programme. The present paper describes the principal goals of LFI, its instrument characteristics and programme. The coordinated use of the two different instrument technologies and analyses of their output data will allow optimal control and suppression of systematic effects, including discrimination of astrophysical sources. All the LFI channels and four of the HFI channels will be sensitive to linear polarization of the CMB. While HFI is more sensitive and should achieve slightly better angular resolution, the combination of the two instruments is required to accurately subtract Galactic emission thereby allowing a reconstruction of the primordial CMB anisotropies to high precision.

LFI (see (Bersanelli et al. 2009) for more details) consists of an array of 11 corrugated horns feeding 22 polarisation-sensitive (see (Leahy et al. 2009) for more details) pseudo-correlation radiometers based on HEMT transistors and MMIC technology which are actively cooled down to 20 K by a new concept sorption cooler specifically designed to deliver high efficiency, long duration cooling power (Wade et al. 2000; Bhandari et al. 2004; Morgante et al. 2009b). A differential scheme for the radiometers is adopted in which the signal from the sky is compared with a stable reference load at $\sim$ 4K (Valenziano et al. 2009). The radiometers cover three frequency bands centred at 30 GHz, 44 GHz, and 70 GHz. The design of the radiometers has been driven by the need to minimize the introduction of systematic errors and suppress noise fluctuations generated in the amplifiers. Originally, LFI was to include seventeen 100 GHz horns with 34 high sensitivity radiometers. This system, which could have granted redundancy and cross calibration with HFI as well as cross check of systematics, was not implemented.

The design of the horns is optimized for achieving beams with the highest resolution in the sky together with the lowest side lobes. Typical LFI main beams have full width half maximum (FWHM) resolutions of about $33'$, $27'$, and $13'$, respectively at 30 GHz, 44 GHz, and 70 GHz, slightly better than the requirements listed in Table 1 for the cosmological oriented 70 GHz channel. The beams are approximately elliptical with ellipticity ratio (i.e. major/minor axis) of $\simeq 1.15 - 1.40$. The beam profiles will be measured in flight by observing planets and strong radio sources (Burigana et al. 2001).

A summary of the LFI performance requirements adopted to drive the instrument design is reported in Table 1.

The constraints on thermal behavior required to minimize systematic effects dictated a Planck cryogenic architecture that is one of the most complicated ever conceived for space. Moreover, the spacecraft has been designed to exploit the favourable thermal conditions of the L2 orbit. The thermal system is a combination of passive and active cooling: passive radiators are used as thermal shields and pre-cooling stages, while active cryocoolers are used both for instruments cooling and pre-cooling. The cryochain consists of the following main sub-systems (Collaudin & Passvogel 1999):

- pre-cooling from 300 K to about 50 K by means of passive radiators in three stages ($\sim$150 K, $\sim$100 K, $\sim$50 K), which are called V-Grooves due to their conical shape;
- cooling to 18 K for LFI and pre-cooling the HFI 4 K cooler via a H_2 Joule-Thomson Cooler with sorption compressors (the Sorption Cooler);
- cooling to 4 K for pre-cooling the HFI dilution refrigerator and for the LFI reference loads via a Helium Joule-Thomson cooler with mechanical compressors;
- cooling of the HFI to 1.6 K and finally 0.1 K with an open loop ^{4}He-^{3}He dilution refrigerator.

The LFI front end unit is maintained at its operating temperature by the Planck H_2 Sorption Cooler Sub-system (SCS): a closed-cycle vibration-free continuous cryocooler designed to provide 1.2 Watt of cooling power at a temperature of 18 K. Cooling is achieved by hydrogen compression, expansion through a Joule-Thomson valve and liquid evaporation at the cold stage. The Planck SCS is the first long-duration system of its kind to be flown on a space platform. Operations and performance are described in more detail in Sect. 3.3 and in Morgante et al. (2009b).

Planck is a spinning satellite. Thus, its receivers will observe the sky through a sequence of (almost great) circles following a scanning strategy (SS) aimed at minimizing systematic effects and achieving all-sky coverage for all receivers. Several parameters are relevant for the SS. The main one is the angle, α, between the spacecraft spin axis and the telescope optical axis. Given the extension of the focal plane unit, each beam centre points to its specific angle, α_r. The angle α is set to 85° to achieve a nearly all-sky coverage even in the so-called *nominal* SS in which the spacecraft spin axis is kept always exactly along the antisolar direction. This choice avoids the "degenerate" case $\alpha_r = 90°$, characterized by a concentration of the crossings of scan circles only at the ecliptic poles and the consequent degradation of the quality of destriping and map making codes (Burigana et al. 1997; Maino et al. 1999; Wright et al. 1996; Janssen & Gulkis 1992). Since the Planck mission is designed to minimize straylight contamination from the Sun, Earth, and Moon (Burigana et al. 2001; Sandri et al. 2009), it is possible to introduce modulations of the spin axis from the ecliptic plane to maximize the sky coverage

Table 1. LFI performance requirements. The average sensitivity per 30' pixel or per FWHM^2 resolution element (δT and δT/T, respectively) is given in CMB temperature (i.e. equivalent thermodynamic temperature) for 14 months of integration. The white noise per frequency channel and 1 sec of integration in given in antenna temperature. See Table 2 and 6 for LFI measured performance.

Frequency channel	30GHz	44GHz	70GHz
InP detector technology	MIC	MIC	MMIC
Angular resolution [arcmin]	33	24	14
δT per 30' pixel [μK]	8	8	8
δT/T per pixel [μK/K]	2.67	3.67	6.29
Number of radiometers (or feeds)	4 (2)	6 (3)	12 (6)
Effective bandwidth [GHz]	6	8.8	14
System noise temperature [K]	10.7	16.6	29.2
White noise per ν channel [μK $\cdot \sqrt{\text{s}}$]	116	113	105
Systematic effects [μK]	< 3	< 3	< 3

[1] Planck (http://www.esa.int/Planck) is a project of the European Space Agency - ESA - with instruments funded by ESA member states (in particular the PI countries: France and Italy), and with special contributions from Denmark and NASA (USA).

keeping constant the solar aspect angle of the spacecraft for thermal stability. This drives us towards the adopted *baseline* SS [2] (Maris et al. 2006a). Thus, the baseline SS adopts a cycloidal modulation of the spin axis, i.e. a precession around a nominal antisolar direction with a semiamplitude cone of 7.5°. In such a way all Planck receivers will cover the whole sky. A cycloidal modulation with a 6 month period satisfies the mission operational constraints while avoiding sharp gradients in the pixel hit count (Dupac & Tauber 2005). Furthermore, this solution allows one to spread the crossings of scan circles in a wide region which is beneficial to map making, particularly for polarization (Ashdown et al. 2007). The last three SS parameters are: the sense of precession (clockwise or anticlockwise), the initial spin axis phase along the precession cone, and, finally, the spacing between two consecutive spin axis repointings, chosen at 2′ to achieve four all-sky surveys with the available guaranteed number of spin axis manoeuvres.

LFI is the result of an active collaboration among about a hundred universities and research centres, in Europe, Canada and USA, organized in the LFI Consortium (supported by more than 300 scientists) funded by national research and space agencies. The Principal Investigator leads a team of 26 Co-Investigators responsible for the development of the instrument hardware and software. The hardware has been developed under the supervision of an Instrument Team. The data analysis and its scientific exploitation are mostly carried out by a Core Team of about 100 scientists, working in close connection with the Data Processing Centre (DPC). The Core Team is closely linked to a Planck wider scientific community, comprising, other than LFI, the HFI and Telescope Consortia, organized in a structure of Working Groups. Planck is managed by the ESA Planck Science Team.

The paper is organized as follows. In section 2 we report the LFI cosmological and astrophysical objectives and role in the overall mission. A certain attention is there devoted to compare LFI and WMAP sensitivities to the CMB angular power spectrum in almost common frequency bands and to discuss the cosmological improvement with respect to WMAP from LFI alone and in combination with HFI. Section 3 is devoted to the LFI optics, radiometers and Sorption Cooler set up and performance. The LFI programme is set forth in Section 4. LFI Data Processing Centre is illustrated in Section 6 following a report on the LFI tests and verifications in Section 5. Conclusions are drawn in Section 7.

2. Cosmology and astrophysics with LFI and Planck

Planck is the third generation space mission for CMB anisotropies and will open a new era in the understanding of the Universe (The Planck Collaboration 2006). It will measure cosmological parameters with a much greater level of accuracy than all previous efforts. Furthermore, Planck's high resolution all-sky survey, the first ever in the microwave range, will provide a legacy to the astrophysical community for years to come.

2.1. Cosmology

The LFI instrument will play a crucial role for cosmology. Its LFI 70 GHz channel is in a frequency window remarkably clear from foreground emissions, making it particularly advantageous to observe both CMB temperature and polarization. The two lower frequency channels at 30 GHz and 44 GHz will accurately monitor Galactic and extra-Galactic foreground emissions (see Sect. 2.2) whose removal (see Sect. 2.3) as is critical for the a successful mission. This aspect is of key importance for CMB polarization measurements since Galactic emission dominates the polarized sky.

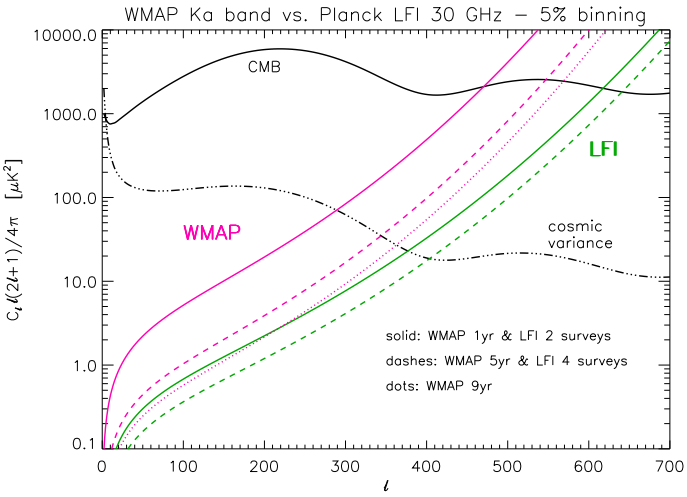

Figure 1. CMB temperature anisotropy APS (black solid line) compatible with WMAP data is compared to WMAP (Ka band) and LFI (30 GHz) sensitivity to the APS (Knox 1995), assuming subtracted the noise expectation, for different integration times as reported in the figure. The plot reports separately the cosmic variance (black three dot-dashes) and the instrumental noise (red and green lines for WMAP and LFI, respectively) assuming a multipole binning of 5%. Regarding sampling variance, an all-sky survey is assumed here for simplicity. The use of the CAMB code is acknowledged (http://camb.info/).

The full exploitation of the cosmological information contained in CMB maps will be largely based on the joint analysis of LFI and HFI data. While a complete discussion of this aspect is out of the scope of this paper, in the next subsections we will discuss some topics of particular relevance for LFI or for a combined analysis of LFI with HFI data. In Subsect. 2.1.1 we will review the LFI sensitivity to the angular power spectrum on the basis of the realistic LFI sensitivity (see Table 6) and resolution (see Table 3.1) derived from extensive tests. This instrument description is adopted in Subsect. 2.1.2 to estimate the LFI accuracy in the extraction of a representative set of cosmological parameters, alone and in combination with HFI. Subsect. 2.1.3 addresses the problem of the detection of primodial non-Gaussianity, a topic, of particular interest for the LFI Consortium, that will largely take advantage from the combination of LFI and HFI since the necessity of catching with foregrounds. At large angular scales, WMAP shown a minimum of the foreground in the V band, thus we expect that the LFI 70 GHz channel will be of particular interest for investigation of the CMB pattern at large scales, a topic discussed in Subsect. 2.1.4.

2.1.1. Sensitivity to CMB angular power spectra

The statistical information encoded in CMB anisotropies, in both temperature and polarization, can be analyzed in terms of a "compressed" estimator, the angular power spectrum (APS). Provided that the CMB anisotropies obey Gaussian statistics, as predicted in a wide class of models, the APS contains most of the relevant statistical properties. The quality of the recovered APS

[2] The above nominal SS is kept as backup solution in the case of a possible verification in flight of an unexpected, bad behaviour of Planck optics.

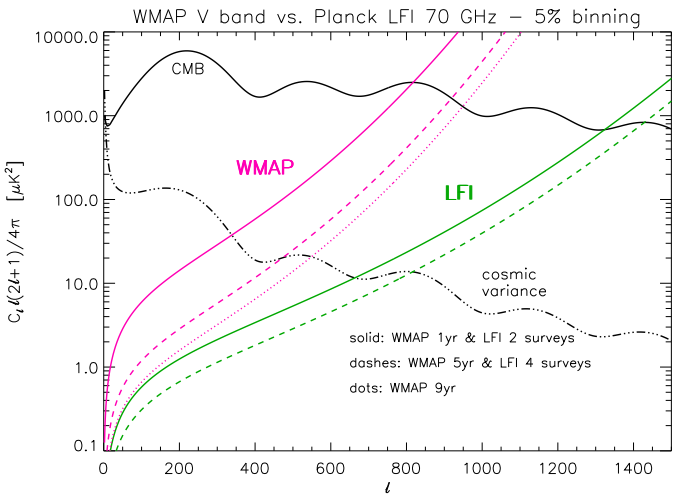

Figure 2. As in Fig. 1 but for the sensitivity of WMAP in V band and LFI at 70 GHz.

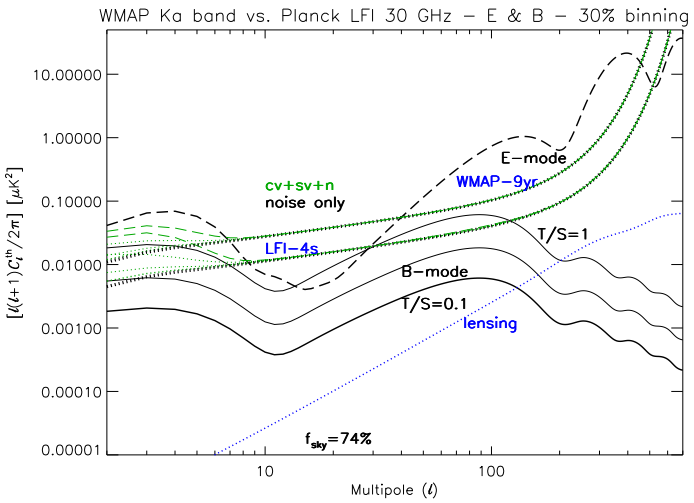

Figure 3. CMB E polarization modes (black long dashes) compatible with WMAP data and CMB B polarization modes (black solid lines) for different tensor-to-scalar ratios of primordial perturbations ($r = T/S = 1, 0.3, 0.1$, at increasing thickness; $r = T/S$ is defined here in the Fourier space) are compared to WMAP (Ka band, 9 years of observations) and LFI (30 GHz, 4 surveys) sensitivity to the APS (Knox 1995), assuming subtracted the noise expectation. The plots include cosmic and sampling variance plus instrumental noise (green dots for B modes, green long dashes for E modes, labeled with cv+sv+n; black thick dots, noise only) assuming a multipole binning of 30%. Note that the cosmic and sampling (74% sky coverage) variance implies a dependence of the overall sensitivity at low multipoles on r (again the green lines refer to $r = 1, 0.3, 0.1$, from top to bottom), which is relevant for parameter estimation; instrumental noise only determines capability to detect the B mode. The B mode induced by lensing (blue dots) is shown for comparison.

is a good predictor of the efficiency in extracting cosmological parameters through a comparison with theoretical predictions arising from Boltzmann codes. Strictly speaking, the latter task must be carried out through likelihood analyses. Neglecting systematic effects (and correlated noise), the sensitivity of a CMB anisotropy experiment to APS, C_ℓ, at each multipole ℓ is summarized by the equation (Knox 1995)

$$\frac{\delta C_\ell}{C_\ell} \simeq \sqrt{\frac{2}{f_{\rm sky}(2\ell+1)}}\left[1+\frac{A\sigma^2}{NC_\ell W_\ell}\right], \quad (1)$$

where A is the size of the surveyed area, $f_{\rm sky} = A/4\pi$, σ is the rms noise per pixel, N is the total number of observed pixels, and W_ℓ is the beam window function. For a symmetric Gaussian beam $W_\ell = \exp(-\ell(\ell+1)\sigma_{\rm B}^2)$ where $\sigma_{\rm B} = {\rm FWHM}/\sqrt{8\ln 2}$ defines the beam resolution.

Even in the limit of an experiment with infinite sensitivity ($\sigma = 0$) the accuracy on the APS is limited by the so-called cosmic and sampling variance, reducing to pure cosmic variance in the case of all-sky coverage, which is quite relevant at low ℓ because of the relatively small number of available modes m per multipole in the spherical harmonic expansion of a sky map. The multifrequency maps to be obtained with Planck will allow one to improve the foreground subtraction and maximize the effective sky area used in the APS analysis, thus improving upon the understanding of the CMB APS obtained from previous experiments. Anyway, the main benefits of the improved foreground subtraction come in polarization and for non-Gaussianity test.

Figs. 1 and 2 compare WMAP [3] and LFI [4] sensitivity to the APS of CMB temperature anisotropies at two similar frequency bands displaying separately the uncertainty coming from cosmic variance and instrumental performance and considering different project lifetimes. For ease of comparison, we consider the same multipole binning (in both cosmic variance and instrumental sensitivity). The figures show how the multipole region where cosmic variance dominates over instrumental sensitivity moves to higher multipoles in the case of LFI and that the LFI 70 GHZ channel allows us to extract information on about two additional acoustic peaks with respect to those achievable with the corresponding WMAP V band.

A somewhat similar comparison is shown in Figs. 3 and 4 but for the E and B polarization modes considering in this case only the longest mission lifetimes (9 yrs for WMAP, 4 surveys for Planck) reported in previous figures and a larger multipole binning: note the increase in signal-to-noise ratio. Clearly, foregrounds are much more critical to measurements of polarization than they are to measurements of temperature. At the WMAP V band and the LFI 70 GHz channels the polarized foreground is minimal (at least considering a very large sky fraction and up to the range of multipoles already explored by WMAP). Thus, we consider these optimal frequencies to show the potential uncertainty expected from polarized foregrounds. While the Galactic foreground dominates over the CMB B mode and also over the CMB E mode up to multipoles of several tens, a foreground subtraction at 5–10% accuracy of the map level is enough to reduce residual Galactic contamination to well below the CMB E mode and below the CMB B mode for a wide range of multipoles typically for $r = T/S \lesssim 0.3$ (r is defined in the Fourier space). If we are able to model Galactic polarized foregrounds at several % accuracy, at the LFI 70 GHz channel the main limitation will come from the instrumental noise. This will prevent an accurate E mode evaluation at $\ell \sim 7-20$, or a B mode detection for $r \lesssim 0.3$. Clearly, a better recovery of the APS polarization modes will come from the exploitation of the Planck data at all frequencies and in this context LFI data will be crucial to better model the polarized synchrotron emission which is necessary to remove at some % accuracy (or better) at map level to be able

[3] http://lambda.gsfc.nasa.gov/

[4] In this comparison, we exploit realistic LFI optical and instrumental performance as described in the following sections.

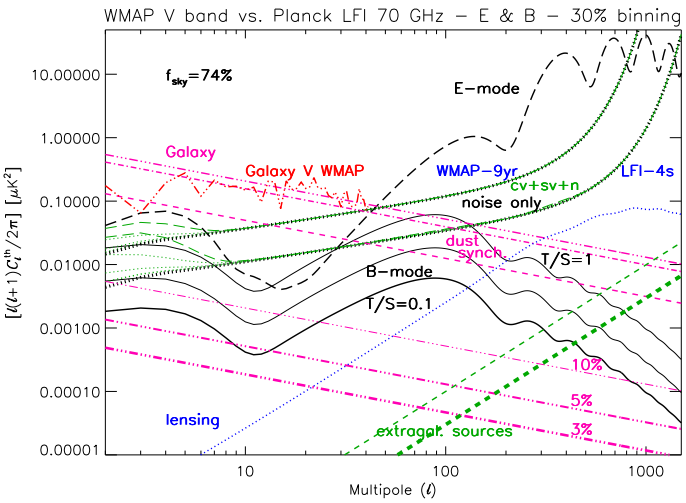

Figure 4. As in Fig. 3 but for the sensitivity of WMAP in V band and LFI at 70 GHz, and including also the comparison with Galactic and extragalactic polarized foregrounds. Galactic synchrotron (purple dashes) and dust (purple dot-dashes) polarized emissions produce the overall Galactic foreground (purple three dot-dashes). WMAP 3-yr power-law fits for uncorrelated dust and synchrotron have been used. For comparison, WMAP 3-yr results derived directly with the HEALPix package (http://healpix.jpl.nasa.gov/, Górski et al. (2005)) from the foreground maps are shown on a suitable multipole range: power-law fits provide (generous) upper limits for the power at low multipoles. (For simplicity, we report here only the WMAP results found for the Galactic B mode, that are different from those found for the E mode, but much less remarkably than for the case of CMB modes). Residual contaminations by Galactic foregrounds (purple three dot-dashes) are shown for 10%, 5%, and 3% of the map level, at increasing thickness, as labeled in the figure. The residual contribution by unsubtracted extragalactic sources, $C_\ell^{\rm res,PS}$ and the corresponding uncertainty, $\delta C_\ell^{\rm res,PS}$ computed assuming a relative uncertainty $\delta\Pi/\Pi = \delta S_{\rm lim}/S_{\rm lim} = 10\%$ in the knowledge of their degree of polarization and in the determination of the source detection threshold, are also plotted as green dashes, thin and thick, respectively.

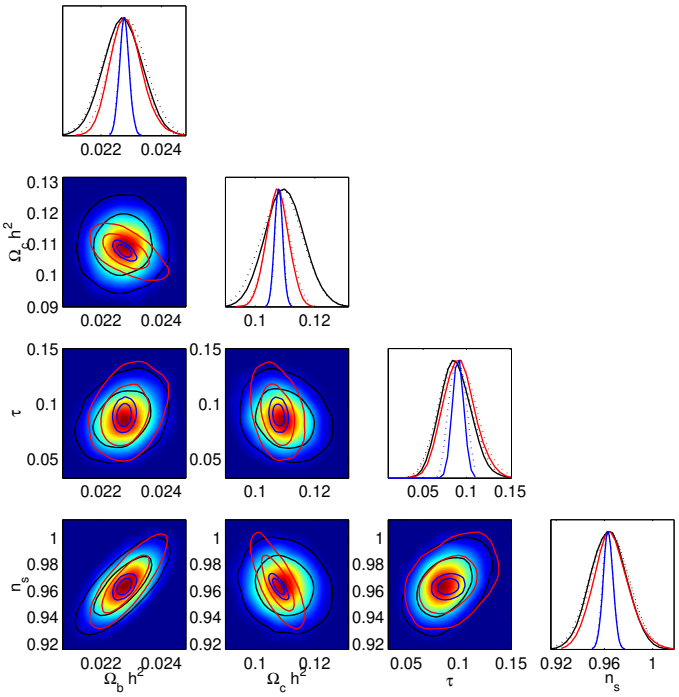

Figure 5. Forecasts of 1σ and 2σ contours for the cosmological parameters of the WMAP5 best-fit ΛCDM cosmological model with reionization as expected from Planck (blue lines) and from LFI alone (red lines) after 14 months of observations. The black contours are those obtained from WMAP five years observations. See the text for more details.

to detect primordial B modes for $r \lesssim 0.1$ (Efstathiou & Gratton 2009).

2.1.2. Cosmological parameters

Given the improvement over the WMAP APS recovery achievable with the better sensitivity and resolution of Planck (as discussed in the previous section for LFI), a correspondingly better determination of cosmological parameters is expected. Of course, the better sensitivity and angular resolution of HFI channels compared to WMAP and LFI ones will largely contribute to the improvement on cosmological parameters expected by Planck.

We present here the comparison between the determinations of a suitable set of cosmological parameters with data from WMAP, Planck, and Planck LFI alone.

In Fig. 5 we compare the forecasts for 1σ and 2σ contours for 4 cosmological parameters of the WMAP5 best-fit ΛCDM cosmological model (with reionization parametrized by the Thomson optical depth τ) expected from the Planck LFI 70 GHz channel alone after 14 months of observations (red lines), the Planck combined sensitivity for the 70 GHz, 100 GHz, and 143 GHz channels for the same integration time (blue lines), and the WMAP five year observations (black lines). We have taken the 70 GHz channels and the 100 GHz and 143 GHz as the representative channels for LFI and HFI (note that for HFI we have used angular resolution and sensitivities as given in Table 1.3 of the Planck Scientific Programme prepared by The Planck Collaboration (2006),) for cosmological purposes, respectively, and we assumed a coverage of 85% of the sky. Fig. 5 shows that HFI 100 GHz and 143 GHz channels are crucial to obtain the best cosmological parameter determination.

While we have not explicitly considered the other channels of LFI – 30 GHz and 44 GHz – and HFI – at frequencies ≥ 217 GHz – note that they are essential to achieve accurate separation of the CMB from astrophysical emissions, particularly for polarization.

The improvement in cosmological parameters precision from LFI (2 surveys) compared to WMAP 5 is clear from Fig. 5. This is maximized for the dark matter abundance Ω_c due to the better performance of the LFI 70 GHz channel with respect to WMAP 5. From Fig. 5 it is clear that the expected improvement from Planck in cosmological parameters determination compared to that of WMAP 5 can open a new stage in our understanding of cosmology.

2.1.3. Primordial non-Gaussianity

Planck total intensity and polarization data will either provide the first actual meaurement of non-Gaussianity (NG) in the primordial curvature perturbations, or tighten the existing constraints, based on WMAP data, by almost an order of magnitude.

Probing primordial NG is another activity that requires foreground cleaned maps. Hence, the frequency maps of both instruments must be used for this purpose.

A very important feature is that the primordial NG is *model dependent*. As a consequence of the assumed flatness of the

inflaton potential any intrinsic NG generated during standard single-field slow-roll inflation is generally small, hence adiabatic perturbations originating from quantum fluctuations of the inflaton field during standard inflation are nearly Gaussian distributed. Despite the simplicity of the inflationary paradigm, however, the mechanism by which perturbations are generated is not yet fully established and various alternatives to the standard scenario have been considered. Non-standard scenarios for the generation of primordial perturbations in single-field or multi-field inflation indeed allow for greater NG levels. Moreover, alternative scenarios for the generation of the cosmological perturbations like the so-called curvaton, the inhomogeneous reheating and DBI scenarios, are characterized by a potentially large NG level (see e.g. Bartolo et al. (2004) for a review). For this reason detecting or even just constraining primordial NG signals in the CMB is one of the most promising ways to shed light on the physics of the Early Universe.

In the standard way to parameterize primordial non-Gaussianity, the primordial gravitational potential Φ [5] is written as

$$\Phi = \Phi_L + f_{\rm NL}\left(\Phi_L^2 - \left\langle\Phi_L^2\right\rangle\right) ,$$

where Φ_L is a Gaussian random field and $f_{\rm NL}$ is a dimensionless parameter measuring the expected level of quadratic NG. More generally, the parameter $f_{\rm NL}$ should be replaced by a suitable function, and the product by a (double) convolution. Standard single-field slow-roll inflation produces $f_{NL} \ll 1$, while much larger values of $|f_{\rm NL}|$ are allowed by the non-standard inflationary models mentioned above.

For this reason both a positive measurement of the non-Gaussianity strength $f_{\rm NL}$ or an upper limit on its amplitude would represent a crucial observational discriminant between competing models for primordial perturbation generation. A positive detection of $f_{\rm NL} \sim 10$ would imply that all standard single-field slow-roll models of inflation are ruled out. By contrast, an improvement of the limits on the amplitude of $f_{\rm NL}$ will allow one to strongly reduce the class of non-standard inflationary models allowed by the data, thus providing a unique clue on the fluctuation generation mechanism. At the same time, Planck temperature and polarization data will allow different predictions for the *shape* of non-Gaussianities to be tested. Here, shape of NG essentially refers to the triangle configurations (in harmonic space) yielding the dominant contribution to the angular bispectrum of temperature anisotropies (and polarization). Indeed, it has been shown that the above model, with constant $f_{\rm NL}$ is dominated by so-called "squeezed" triangle configurations, for which one multipole, say ℓ_1, is much smaller than the other two: $\ell_1 \ll \ell_2, \ell_3$. This "local" NG is typical of models which produce the perturbations right after inflation (such as for the curvaton or the inhomogeneous reheating scenarios). So-called DBI inflation models, based on non-canonical kinetic terms for the *inflaton* (the scalar field which drives inflation), lead to non-local forms of NG, which are dominated by equilateral triangle configurations: $\ell_1 \approx \ell_2 \approx \ell_3$. Recently, it has been pointed out (Holman & Tolley (2008)) that excited initial states for the inflaton may lead to a third shape, called "flattened" triangle configuration. Thus, the shape information provides another important test for the physical mechanism which generated the initial seeds of CMB anisotropies and large-scale structure formation.

The strongest available CMB limits on $f_{\rm NL}$ for local NG comes from WMAP 5-yr data. In particular, Smith et al. (2009) have obtained $-4 < f_{\rm NL} < 80$ at 95% C.L. using the optimal estimator for local NG. Planck total intensity and polarization data will allow to reduce the above window on $|f_{\rm NL}|$ below 10. Indeed, Babich & Zaldarriaga (2004) and Yadav et al. (2007) have shown that a sensitivity to local non-Gaussianity $\Delta f_{\rm NL} \approx 4$ (1 sigma) is achievable with Planck data (having assumed a ΛCDM cosmology). Notice that accurate measurement of E-type polarization will play a relevant role for this result. Note also that the limits that Planck can achieve in this case are very close to those for an "ideal" experiment. Equilateral-shape NG is less strongly constrained at present. The WMAP team (Komatsu et al. 2009) obtained $-151 < f_{\rm NL} < 253$ at 95% C.L.. Also in this case, Planck will have a strong impact on this constraint. Indeed, various authors (Smith & Zaldarriaga (2006); Bartolo & Riotto (2009)) have estimated that Planck data will allow us to reduce the bound on $|f_{\rm NL}|$ down to around 70.

Measuring the primordial non-Gaussianity in CMB data to such levels of precision requires accurate handling of possible contaminants, such as those introduced by instrumental noise, by the use of masks and imperfect foreground and point source removal. These aspects are presently being dealt with by the Planck team, also with the help of synthetic maps of the CMB including primordial NG as well as realistic models for the various contaminants.

2.1.4. Large scale anomalies

Observations of CMB anisotropies contributed to the building of the standard cosmological model, also known as ΛCDM concordance model, involving a set of parameters on which CMB observations and other cosmological and astrophysical data sets agree: spatial curvature close to zero; 70% of the cosmic density in the form of dark energy; 20−25% in cold dark matter (CDM); 4−5% in baryonic matter; nearly scale invariant adiabatic, Gaussian primordial perturbations. Although the CMB anisotropy pattern obtained by WMAP is largely consistent with the concordance ΛCDM model, there are some interesting and curious deviations from it, in particular on the largest angular scales. These deviations have been obtained with detailed analyses and can be listed as follows. *1) Lack of power at large scales*. The angular correlation function is found to be uncorrelated (i.e. consistent with 0) for angles larger than 60°. In (Copi et al. 2008, 2007) it has been shown that this event happens only in 0.03% of realizations of the concordance model. The surprisingly low amplitude of the quadrupole term of the angular power spectrum (APS), already found by COBE (Smoot et al. 1992; Hinshaw et al. 1996), has been confirmed by WMAP (Dunkley et al. 2009; Komatsu et al. 2009). *2) Hemispherical asymmetries*. It is found that the power coming separately from the two hemispheres (defined by the ecliptic plane) is too asymmetric (especially at low ℓ) (Eriksen et al. 2004a,b; Hansen et al. 2004). *3) Unlikely alignments of low multipoles*. An unlikely (for a statistically isotropic random field) alignment of the quadrupole and the octupole (Tegmark et al. 2003; Copi et al. 2004; Schwarz et al. 2004; Weeks 2004; Land & Magueijo 2005). Moreover, both quadrupole and octupole align with the CMB dipole Copi et al. (2007). Other unlikely alignments are described in (Abramo et al. 2006; Wiaux et al. 2006; Vielva et al. 2007). *4) Cold Spot*. Vielva et al. (2004) detected a non Gaussian behaviour in the southern hemisphere with a wavelet analysis technique (see also Cruz et al. (2005)).

It is still unknown whether these anomalies are hints of new (and fundamental) physics beyond the concordance model or whether they are simply the residual of some imperfectly

[5] More precisely we refer to Bardeen's gauge-invariant gravitational potential, which is such that the CMB anisotropy $\Delta T/T \to -\Phi/3$ in the pure Sachs-Wolfe limit.

removed astrophysical foreground or systematic effect. Planck data will give a precious contribution not only to refine the cosmological parameters of the standard cosmological model but also to solve the aforementioned puzzles thanks to better foreground removal and control of systematic effects. In particular, the LFI 70 GHz channel will be crucial to this scientific aim, since, as probed by WMAP, the foreground at large angular scales is a minimum in the V band.

2.2. Astrophysics

The accuracy of the extraction of the CMB anisotropy pattern from Planck maps largely relies, particularly in polarization, on the quality of the separation of the *background* signal of cosmological origin from the various *foreground* sources of astrophysical origin that are superimposed onto the maps (see also Sect. 2.3). The scientific case for Planck has been presented by The Planck Collaboration (2006) and foresees a full exploitation of the multifrequency data aimed not only at the extraction of the CMB, but also at the separation and study of each astrophysical component, using Planck data alone or in combination with other data sets. This section provides an update of the scientific case, with particular emphasis on the contribution of the LFI to the science goals.

2.2.1. Galactic Astrophysics

Planck will carry out an all-sky survey of the fluctuations of Galactic emissions at its nine frequency bands. The HFI channels at $\nu \geq 100$ GHz will provide the main improvement with respect to COBE on the Galactic dust emission[6], still poorly known particularly in polarization. However, since Galactic dust emission still dominates over free-free and synchrotron at 70 GHz (see e.g. (Gold et al. 2009) and references therein), LFI will provide crucial information on the low frequency tail of this component. The LFI frequency channels, in particular those at 30 GHz and 44 GHz, will be relevant for the study of the diffuse, significantly polarized synchrotron emission and for the essentially unpolarized free-free emission.

Results from the WMAP lowest frequency channels suggest the presence of a further contribution, probably correlated with dust. While a model with complex synchrotron emission pattern and spectral index cannot be excluded, several interpretations of microwave (see e.g. (Hildebrandt et al. 2007; Bonaldi et al. 2007)) and radio (La Porta et al. 2008) data, and in particular the recent ARCADE 2 results (Kogut et al. 2009), seem to support the identification of this anomalous component as spinning dust (Draine & Lazarian 1998; Lazarian & Finkbeiner 2003). LFI data, in particular at 30 GHz, will shed new light on this intriguing question.

Another intriguing component that will be further addressed by Planck data is the so-called haze emission in the inner Galactic region, possibly generated by synchrotron emission from relativistic electrons and positrons produced in the annihilations of dark matter particles (see e.g. (Hooper et al. 2007; Cumberbatch et al. 2009; Hooper et al. 2008) and references therein).

Furthermore, the full interpretation of the Galactic diffuse emissions in Planck maps will benefit from the joint analysis with radio and far-IR data. For instance PILOT (Bernard et al. 2007) will improve Archeops results (Ponthieu et al. 2005) measuring polarized dust emission at frequencies higher than 353 GHz. Recent all-sky surveys at 1.4 GHz (see e.g. (Burigana et al. 2006) and references therein) and in the range few GHz to 15 GHz will complement the low frequency side (see e.g. PGMS (Haverkorn et al. 2007), C-BASS (Pearson & C-BASS collaboration 2007), QUIJOTE (Rubino-Martin et al. 2008), GEM (Barbosa et al. 2006)) allowing an accurate multifrequency analysis of the depolarization phenomena at low and intermediate Galactic latitudes. The detailed knowledge of the underlying noise properties in Planck maps will allow one to measure the correlation characteristics of diffuse component, greatly improving physical models for the interstellar medium (ISM). The ultimate goal of these studies is the development of a consistent Galactic 3D model, which includes the various components of the ISM, large and small scale magnetic fields (see e.g. Waelkens et al. (2009)), and turbulence phenomena (Cho & Lazarian 2003).

While at moderate resolution and limited in flux to a few hundred mJy, Planck will also provide multifrequency, all-sky information on discrete Galactic sources, from early stages of massive stars to late stages of stellar evolution (Umana et al. 2006), from HII regions (Paladini et al. 2003) to dust clouds (Pelkonen et al. 2007). Models for the enrichment of the ISM and for the interplay between stellar formation and ambient physical properties will be further tested.

Planck will have also a chance to observe some Galactic micro-blazars (like e.g. Cygnus X-3) in a flare phase and perform a multifrequency monitoring of these events on timescales from hours to weeks. A Quick Detection Software (QDS) for the identification of source flux variation, working on Planck time ordered data, has been developed by the Finnish group in collaboration with LFI DPC (Aatrokoski et al. 2009).

Finally, Planck will provide crucial information for modeling the emission from moving objects and diffuse interplanetary dust in the Solar System. The mm and sub-mm emission from planets and up to 100 asteroids will be studied (Cremonese et al. 2002; Maris & Burigana 2009). Moreover the Zodiacal Light Emission will be measured with great accuracy, free from residual Galactic contamination (Maris et al. 2006b).

2.2.2. Extragalactic Astrophysics

The higher sensitivity and better angular resolution of LFI compared to WMAP will allow us to obtain substantially richer samples of extragalactic sources at mm wavelengths. Applying a new multi-frequency linear filtering technique to realistic LFI simulations of the sky, Herranz et al. (2009) detected, with 95% reliability, 1600, 1550, and 1000 sources at 30, 44, and 70 GHz, respectively, over about 85% of the sky. The 95% completeness fluxes are 540, 340, and 270 mJy at 30, 44, and 70 GHz, respectively. For comparison, the total numbers of $|b| > 5^\circ$ sources detected by Massardi et al. (2009) at $\geq 5\sigma$ in WMAP 5-yr maps at 33, 41, and 61 GHz, including several possibly spurious objects, are 307, 301, and 161, respectively; the corresponding detection limits increase from $\simeq 1$ Jy at 23 GHz, to $\simeq 2$ Jy at 61 GHz. The number of detections reported by Wright et al. (2009) is lower by $\simeq 20\%$.

As illustrated by Fig. 6, the much bigger source sample expected from Planck will allow us to have good statistics for different sub-populations of sources, some of which are not or only poorly represented in the WMAP sample. The dominant radio population at LFI frequencies consists of flat-spectrum radio quasars (FSRQs), for which LFI will provide a bright sample

[6] At far-IR frequencies significantly higher than those covered by Planck, much information comes from IRAS (see e.g. (Miville-Deschênes & Lagache 2005) for a recent version of the maps).

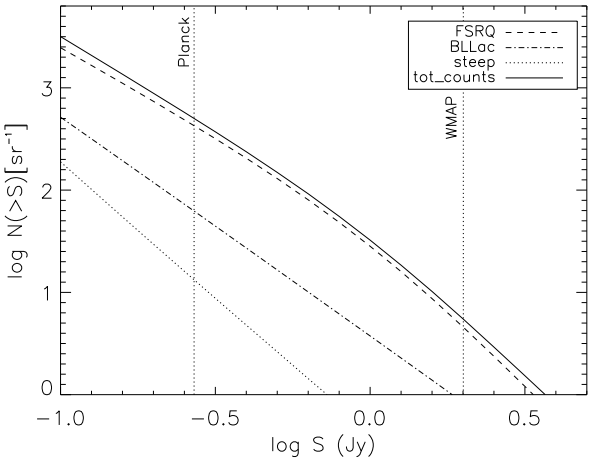

Figure 6. Integral counts of different radio source populations at 70 GHz (flat-spectrum radio quasars, FSRQs; BL Lac objects, steep-spectrum sources), as predicted by the de Zotti et al. (2005) model. The vertical dotted lines show the estimated completeness limits for Planck and WMAP (61 GHz) surveys (see text).

of $\geq$ 1000 objects, well suited to cover the parameter space of current physical models. Interestingly, the expected numbers of blazars and BL Lac objects detectable by LFI are similar to those expected from the Fermi Gamma-ray Space Telescope (formerly GLAST; (Abdo 2009); (Fermi/LAT Collaboration: W.B. Atwood 2009)). It is likely that the LFI and the Fermi blazar samples will have a substantial overlap, making possible a much better definition of the relationships between radio and gamma-ray properties of these sources than has been possible so far. The analysis of spectral properties of the ATCA 20 GHz bright sample indicates that quite a few high-frequency selected sources have peaked spectra. Most of them are likely to be aged beamed objects (blazars) whose radio emission is dominated by a single knot in the jet caught in a flaring phase. The Planck sample will allow us to get key information on the frequency and timescales of such flaring episodes, on the distribution of their peak frequencies, and therefore on the propagation of the flare along the jet. A small fraction of sources showing high frequency peaks may be extreme High Frequency Peakers (Dallacasa et al. 2000), thought to be newly born radio sources (ages as low as thousand years). Obviously, the discovery of just a few such sources would be extremely important to shed light on the poorly understood mechanisms that trigger the radio activity of Galactic cores.

WMAP has detected polarized fluxes at $\geq 4\,\sigma$ in two or more bands for only five extragalactic sources (Wright et al. 2009). LFI will substantially improve on that, providing polarization measurements for tens of sources, thus allowing us to get the first statistically meaningful unbiased sample for polarization studies at mm wavelengths. It should be noted that Planck polarization measurements will not be confusion limited, as in the case of total flux, but noise limited. Thus the detection limit for polarized flux in Planck-LFI channels will be $\simeq$ 200–300 mJy, i.e. lower than for total flux.

As mentioned above, the astrophysics programme of Planck is much wider than that achievable with LFI alone, both for the specific role of HFI and, in particular, for the great scientific synergy between the two instruments. As a remarkable example we mention below the Planck contribution to the astrophysics of clusters. Planck will detect thousands of galaxy clusters out to redshifts of order unity via their thermal Sunyaev-Zeldovich effect (Leach et al. 2008; Bartlett et al. 2008). This sample will be extremely important both to understand the formation of large scale structure and the physics of the intracluster medium. For such measurements, a broad spectral coverage, i.e. the combination of data from both Planck instruments (LFI and HFI), is a key asset. Such a combination, supplemented by ground-based, follow-up observations planned by the Planck team, will allow, in particular, accurate correction for the contamination from radio sources (mostly thanks to LFI channels) and from dusty galaxies (HFI channels) either associated with the clusters or in their foreground/background (Lin et al. 2009).

2.3. Scientific data analysis

Data analysis for a high precision experiment such as LFI must provide reduction of the data volume by several orders of magnitude with minimal loss of information. The sheer size of the dataset, the high sensitivity required to achieve the science goals, and the significance of the statistical and systematic sources of error all conspire to make data analysis an all but trivial task.

The map making layer provides a lossless compression by several orders of magnitude, projecting the dataset from time domain to the discretized celestial sphere (Tegmark 1997; Wright et al. 1996; Lineweaver et al. 1994; Janssen & Gulkis 1992). Furthermore, timeline-specific instrumental effects that are not scan synchronous get reduced in magnitude when projected from time to pixel space (see e.g. Mennella et al. (2002)) and, in general, the analysis of maps provides a more convenient means to assess the level of systematics as compared to timeline analysis.

Several map making algorithms have been proposed to produce sky maps in total intensity (Stokes I) and linear polarization (Stokes Q and U) out of LFI timelines. So-called "destriping" algorithms have historically been proposed first. These take advantage of the details of the Planck scanning strategy to suppress correlated noise (Maino et al. 1999). Although computationally efficient, these methods do not -in general- yield a minimum variance map. To overcome this problem, minimum variance map making algorithms have been devised and implemented specifically for LFI (Natoli et al. 2001; de Gasperis et al. 2005). The latter are also known as Generalized Least Squares (GLS) methods and are accurate and flexible. Their drawback is that, at Planck size, they require a significant amount of massively powered computational resources (Poutanen et al. 2006; Ashdown et al. 2007, 2009) and are thus infeasible to use within a Monte Carlo context. To overcome the limitations of GLS algorithms the LFI community has developed so-called "hybrid" algorithms (Keihänen et al. 2005; Kurki-Suonio et al. 2009; Keihänen et al. 2009). These algorithms rely on a tunable parameter connected to the $1/f$ knee frequency, a measure of the amount of low frequency correlated noise in the time ordered data: the higher the knee frequency, the shorter the "baseline" length that needs to be chosen to properly suppress the $1/f$ contribution. In this view, the GLS solution can be thought of as the limiting case when the baseline length approaches the sampling interval. Provided that the knee frequency is not too high, hybrid algorithm can achieve GLS accuracy at a fraction of the computational demand. Furthermore, they can be tuned to desired precision when speed is an issue (e.g. for timeline to map Monte Carlo production). The baseline map making algorithms for LFI is an hybrid code dubbed `madam`.

Map making algorithms can in general compute the correlation (inverse covariance) matrix of the map estimate they produce (Keskitalo et al. 2009). At high resolution such a compu-

tation, though feasible, is impractical, because the size of the matrix makes its handling and inversion prohibitive. At low resolution the covariance matrix will be produced instead: it is of extreme importance for the accurate characterization of the low multipoles of the CMB (Keskitalo et al. 2009; Gruppuso et al. 2009).

A key tier of Planck data analysis is the separation of astrophysical from cosmological components. A variety of methods have been developed to this end (Leach et al. 2008). Point source extraction is achieved exploiting non-Planck catalogues as well as filtering Planck maps with optimal functions (wavelets) capable of recognizing beam like patterns. In addition to linearly combining the maps or fitting for known templates, diffuse emissions are separated by using the statistical distributions of the different components, assuming independence between them, or by means of a suitable parametrization and fitting of foreground unknowns on the basis of spatial correlations in the data or, in alternative, multi-frequency single resolution elements only.

The extraction of statistical information from the CMB usually proceeds via correlation functions. Since the CMB field is Gaussian to large extent (Smith et al. 2009), most of the information is encoded in the two-point function or equivalently in its reciprocal representation in spherical harmonics space. Assuming rotational invariance, the latter quantity is well described by the APS (see e.g. Gorski (1994)). For an ideal experiment, the estimated APS could be directly compared to a Boltzmann code prediction to constrain the cosmological parameters. However, in view of incomplete sky coverage (which induces couplings among multipoles) and the presence of noise (which, in general, is not rotationally invariant due to the coupling between correlated noise and scanning strategy) a more accurate analysis is necessary. The likelihood function for a Gaussian CMB sky can be easily written and provide a sound mechanism to constrain models and data. The direct evaluation of such a function, however, poses untractable computational issues. Fortunately, only the lowest multipoles require exact treatment. This can be done either by direct evaluation in the pixel domain or sampling the posterior distribution of the CMB using sampling methods such as the Gibbs approach (Jewell et al. 2004; Wandelt et al. 2004). At high multipoles, where the likelihood function cannot be evaluated exactly, a wide range of effective, computationally affordable approximations exist (see e.g. Hamimeche & Lewis (2008) and Rocha et al. (2009) and references therein). The low and high ℓ approaches to power spectrum estimation will be joined into an hybrid procedure, pioneered in Efstathiou (2004).

The data analysis of LFI will require daunting computational resources. In view of the size and complexity of its data set, accurate characterization of the scientific results and errors propagation will be achieved through massive use of Monte Carlo simulations. A number of worldwide distributed supercomputer centres will support the DPC in this activity. A partial list includes NERSC-LBNL in the USA, CINECA in Italy, CSC in Finland and MARE NOSTRUM in Spain. The european centres will benefit of the Distributed European Infrastructure for Supercomputer Application [7].

3. Instrument

3.1. Optics

During the design phase of LFI, great effort was dedicated to the optical design of the focal plane unit. As already mentioned in the Introduction, the actual design of the Planck telescope derives from COBRAS and has been further tuned by the subsequent studies of the LFI team (Villa et al. (1998)) and Thales-Alenia Space. These studies demonstrated the importance of increasing the telescope diameter (Mandolesi et al. (2000)), optimizing the optical design, also showed how complex it would be to match the real focal surface with the horn phase centres (Valenziano et al. (1998)). The optical design of LFI is the result of a long iteration process in which the position and orientation of each feed horn has been optimized as a trade-off between angular resolution and sidelobe rejection levels (Sandri et al. (2004); Burigana et al. (2004); Sandri et al. (2009)). Tight limits were also imposed by mechanical constraints. The 70 GHz system has been subject to a dedicated activity to improve the single horn design and its relative location in the focal surface. As a result the angular resolution has been maximized.

The feed horn development programme started in the early stages of the mission with prototype demonstrators (Bersanelli et al. (1998)), followed by the Elegant Bread Board (Villa et al. (2002)) and finally by the Qualification and Flight Models (Villa et al 2009). The horn design has a corrugated shape with a dual profile (Gentili et al. (2000)). This choice was a posteriori justified by the complexity of the focal plane and the need to respect the interfaces with HFI.

Each of the corrugated horns feeds an orthomode transducer (OMT) which splits the incoming signal into two orthogonal polarized components (D'Arcangelo et al. 2009a). The polarization capabilities of the LFI are guaranteed by the use of OMTs just after the corrugated horns. While the incoming polarization state is preserved inside the horn, the OMT divides it into two linear orthogonal polarizations allowing LFI to measure the linear polarization component of the incoming sky signal. The typical value of OMT cross polarization is about −30dB setting the spurious polarization of the LFI optical interfaces at a level of 0.001.

Table 2 shows the overall LFI optical characteristics as expected in flight (Tauber et al. (2009)). The edge taper (ET) values, quoted in Table 2, refer to the horn taper. They are reference values assumed during the design phase and do not correspond to the real edge taper on the mirrors (see Sandri et al. (2009) for details). The reported angular resolution is the average full width half maximum (FWHM) of all the channels at the same frequency. The cross polar discrimination (XPD) is the ratio between the antenna solid angle of the cross polar pattern and the antenna solid angle of the copolar pattern, both calculated within the solid angle of the −3dB contour. The Sub and Main reflector spillovers are the fraction of power that reaches the horns without being intercepted by the main and sub reflectors respectively.

Table 2. LFI Optical performance. All the values are averaged over all channels at the same frequency. ET is the horn edge taper measured at 22° from the horn axis; FWHM is the angular resolution in arcmin; e is the ellipticity; XPD is the cross polar discrimination in dB; Ssp is the Sub reflector spillover (%); Msp is the Main reflector spillover (%). See text for details.

	ET	FWHM	e	XPD	Ssp	Msp
70	17dB @22°	13.03	1.22	-34.73	0.17	0.65
44	30dB @22°	26.81	1.26	-30.54	0.074	0.18
30	30dB @22°	33.34	1.38	-32.37	0.24	0.59

[7] www.deisa.eu

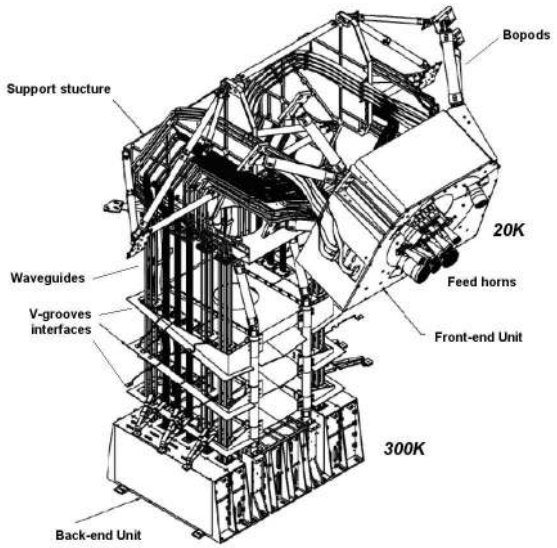

Figure 7. The LFI radiometer array assembly, with details of the front-end and back-end units. The front-end radiometers are based on wide-band low-noise amplifiers, fed by corrugated feedhorns which collect the radiation from the telescope. A set of compsite waveguides transport the amplified signals from the front-end unit (at 20 K) to the back-end unit (at 300 K). The waveguides are designed to meet simultaneously radiometric, thermal, and mechanical requirements, and are thermally linked to the three V-Groove thermal shields of the Planck payload module. The back-end unit, located on top of the Planck service module, contains additional amplification as well as the detectors, and is interfaced to the data acquisition electronics. The HFI is inserted into and attached to the frame of the LFI focal-plane unit.

3.2. Radiometers

LFI is designed to cover the low frequency portion of the wide-band Planck all-sky survey. A detailed description of the design and implementation of the LFI instrument is given in Bersanelli et al. (2009) and references therein, while the results of the on-ground calibration and test campaign is presented in Mennella et al. (2009) and Villa et al. (2009b). The LFI is an array of cryogenically cooled radiometers designed to observe in three frequency bands centered at 30 GHz, 44 GHz, and 70 GHz with high sensitivity and freedom from systematic errors. All channels are sensitive to the I, Q and U Stokes parameters thus providing information on both temperature and polarisation anisotropies. The heart of the LFI instrument is a compact, 22-channel multifrequency array of differential receivers with cryogenic low-noise amplifiers based on indium phosphide (InP) high-electron-mobility transistors (HEMTs). To minimise power dissipation in the focal plane unit, which is cooled to 20 K, the radiometers are split into two subassemblies (the front-end module, FEM, and back-end module, BEM) connected by a set of composite waveguides, as shown in Figure 7. Miniaturized, low-loss passive components are implemented in the front end for optimal performance and for compatibility with the stringent thermo-mechanical requirements in the interface with the HFI.

The radiometer design is driven by the need to suppress $1/f$-type noise induced by gain and noise temperature fluctuations in the amplifiers, which would be unacceptably high for a simple total power system. A differential pseudo-correlation scheme is adopted, in which signals from the sky and from a blackbody reference load are combined by a hybrid coupler, amplified in two independent amplifier chains, and separated out by a second

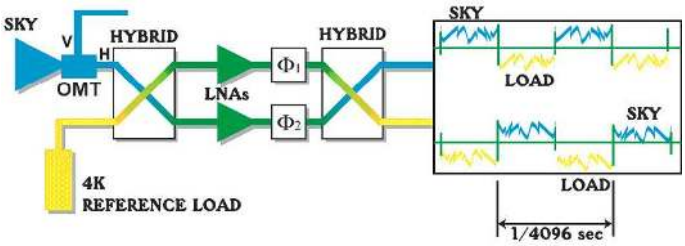

Figure 8. Schematic of the LFI front-end radiometer. The front-end unit is located at the focus of the Planck telescope, and comprises: dual profiled corrugated feed horns; low-loss (0.2 dB), wideband (> 20%) orthomode transducers; and radiometer front-end modules with hybrids, cryogenic low noise amplifiers, and phase switches. For details see (Bersanelli et al. 2009).

hybrid (Figure 8). The sky and the reference load power can then be measured and differenced. Since the reference signal has been subject to the same gain variations in the two amplifier chains as the sky signal, the sky power can be recovered with high precision. Insensitivity to fluctuations in the back-end amplifiers and detectors is realized by switching phase shifters at 8 kHz synchronously in each amplifier chain. The rejection of $1/f$ noise as well as the immunity to other systematic effects is optimised if the two input signals are nearly equal. For this reason the reference loads are cooled to 4 K (Valenziano et al. 2009) by mounting them on the 4 K structure of the HFI. In addition, the effect of the residual offset (< 1 K in nominal conditions) is reduced by introducing a gain modulation factor in the on-board processing to balance the output signal. As shown in Figure 8, the differencing receiver greatly improves the stability of the measured signal (see also Fig. 8 in Bersanelli et al. (2009)).

The LFI amplifiers at 30 GHz and 44 GHz use discrete InP HEMTs incorporated into a microwave integrated circuit (MIC). At these frequencies the parasitics and uncertainties introduced by the bond wires in a MIC amplifier are controllable and the additional tuning flexibility facilitates optimization for low noise. At 70 GHz there will be twelve detector chains. Amplifiers at these frequencies will use monolothic microwave integrated circuits (MMICs), which incorporate all circuit elements and the HEMT transistors on a single InP chip. At these frequencies, MMIC technology provides not only significantly better performance than MIC technology, but also allows faster assembly and smaller sample-to-sample variance. Given the large number of amplifiers required at 70 GHz, MMIC technology can rightfully be regarded as enabling for the LFI.

Fourty-four waveguides connect the LFI front-end unit, cooled to 20 K by a hydrogen sorption cooler, to the back-end unit, which is mounted on the top panel of the Planck SVM and it is maintained at a temperature of 300 K. The BEU comprises the eleven BEMs and the data acquisition electronics (DAE) unit which provides adjustable bias to the amplifiers and phase switches as well as scienctific signal conditioning. In the back-end modules the the RF signals are further amplified in the two legs of the radiometers by room temperature amplifiers. The signals are then filtered and detected by square law detector diodes. A DC amplifier then boosts the signal output which is connected to the data acquisition electronics. After on-board processing, provided by the Radiometer Box Electronics Assembly (REBA), the compressed signals are downlinked to the ground station together with housekeeping data. The sky and reference load DC signals are transmitted to the ground as two separated streams of data to ensure optimal calculation of the gain modulation factor for minimal $1/f$ noise and systematic effects. The complexity

of the LFI system called for a highly modular plan for testing and integration. Performance verification was first carried out at single unit-level, followed by campaigns at sub-assembly and instrument level, then completed with full functional tests after integration in the Planck satellite. Scientific calibration has been carried out in two main campaigns, first on the individual radiometer chain assemblies (RCAs), i.e. the units comprising a feed horn and the two pseudo-correlation radiometers connected to each arm of the orthomode transducer (see Figure 8), and then at instrument level. For the RCA campaign we used sky loads and reference loads cooled near 4 K which allowed us accurate verification of the instrument performance in near-flight conditions. Instrument level tests were carried out with loads at 20 K, which allowed us to verify the radiometer performance in the integrated configuration. Testing at RCA and Instrument level, both for the qualification model (QM) and for the flight model (FM), were carried out at Thales Alenia Space, Vimodrone (Milano, Italy). Finally, system-level tests of the LFI integrated with HFI in the Planck satellite were carried out at CSL in the summer of 2008.

3.3. Sorption Cooler

The Sorption Cooler Sub-system (SCS) is the first active element of the Planck cryochain. Its purpose is to cool the LFI radiometers down to their operational temperature around 20 K while providing a pre-cooling stage for the HFI cooling system: a 4.5 K mechanical Joule-Thomson cooler and a Benoit style open cycle dilution refrigerator. Two identical sorption coolers have been fabricated and assembled by Jet Propulsion Laboratory (JPL) under a contract with NASA. JPL has been a pioneer in the development and application of such cryo-coolers for space and the two Planck units are the first continuous closed cycle hydrogen sorption coolers to be used for a space mission (Morgante et al. 2009b).

Sorption refrigerators are attractive systems for cooling instruments, detectors and telescopes when a vibration free system is required. Since pressurization and evacuation is accomplished simply by heating and cooling the sorbent elements sequentially, with no moving parts, they tend to be very robust and, essentially, generate no vibrations on the spacecraft. This provides excellent reliability and long life. Also, cooling by Joule-Thomson (J-T) expansion through orifices, the cold end can be located remotely (thermally and spatially) from the warm end. This allows for excellent flexibility in integration of the cooler to the cold payload and the warm spacecraft.

3.3.1. Specifications

The main requirements of the Planck SCS can be summarized below:

- Provide about 1 W total heat lift at instrument interfaces using a ≤ 60 K pre-cooling temperature at the coldest V-Groove radiator on the Planck spacecraft
- Maintain the following instrument interfaces temperatures:
  - LFI at ≤ 22.5 K [80% of total heat lift]
  - HFI at ≤ 19.02 K [20% of total heat lift]
- Temperature stability (over one full cooler cycle ≈ 6000 s):
  - ≤ 450 mK, peak-to-peak at HFI interface
  - ≤ 100 mK, peak-to-peak at LFI Interface
- Input power consumption ≤ 470 W (at end of life, excluding electronics)
- Operational lifetime: ≥ 2 years (including testing)

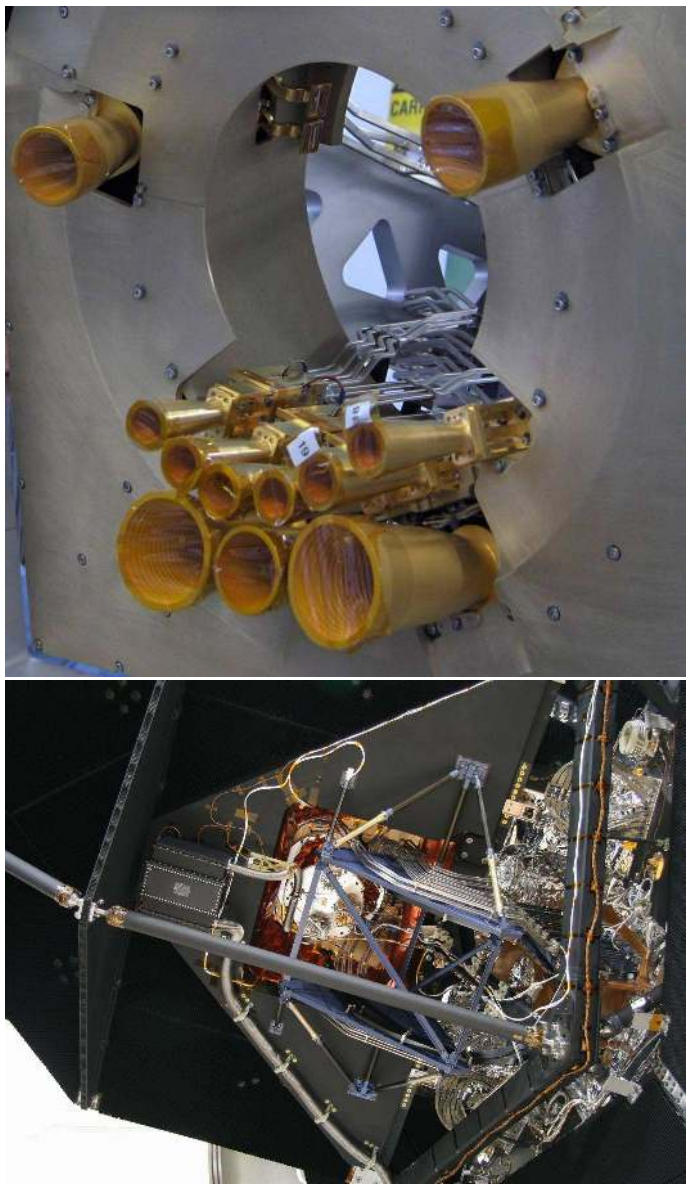

Figure 9. Top panel: picture of the LFI focal plane showing the feed-horns and main frame. The central portion of the main frame is designed to provide the interface to the HFI front-end unit, where the reference loads for the LFI radiometers are located and cooled to 4K. Bottom panel: A back-view of the LFI integrated on the Planck satellite. Visible are the upper sections of the waveguides interfacong the front-end unit, as well as the mechanical support structure.

3.3.2. Operations

The SCS is composed of a Thermo-Mechanical Unit (TMU, see Fig. 10) and electronics to operate the system. Cooling is produced by J-T expansion with hydrogen as the working fluid. The key element of the 20 K sorption cooler is the Compressor, an absorption machine that pumps hydrogen gas by thermally cycling six compressor elements (sorbent beds). The principle of operation of the sorption compressor is based on the properties of a unique sorption material (a La, Ni and Sn alloy), which can absorb a large amount of hydrogen at relatively low pressures, and desorb it to produce high-pressure gas when heated in a limited volume. Electrical resistances accomplish heating of the sorbent while the cooling is achieved by thermally connecting, via gas-gap thermal switches, the compressor element

to a warm radiator at 270 K on the satellite Service Module (SVM). Each sorbent bed is connected to both the high pressure and low-pressure sides of the plumbing system through check valves, which allow gas flow in a single direction only. To damp out oscillations on the high-pressure side of the compressor, a High-Pressure Stabilization Tank (HPST) system is utilized. On the low-pressure side, a Low-Pressure Storage Bed (LPSB) filled with hydride, primarily operates as a storage bed for a large fraction of the H_2 inventory required to operate the cooler during flight and ground testing while minimizing the pressure in the non-operational cooler during launch and transportation. The compressor assembly mounts directly onto the Warm Radiator (WR) on the spacecraft. As each sorbent bed is taken through four steps (heat up, desorption, cool-down, absorption) in a cycle, it will intake low-pressure hydrogen and output high-pressure hydrogen on an intermittent basis. In order to produce a continuous stream of liquid refrigerant the sorption beds phases are staggered so that at any given time, one is desorbing while the others are heating up, cooling down, or reabsorbing low-pressure gas.

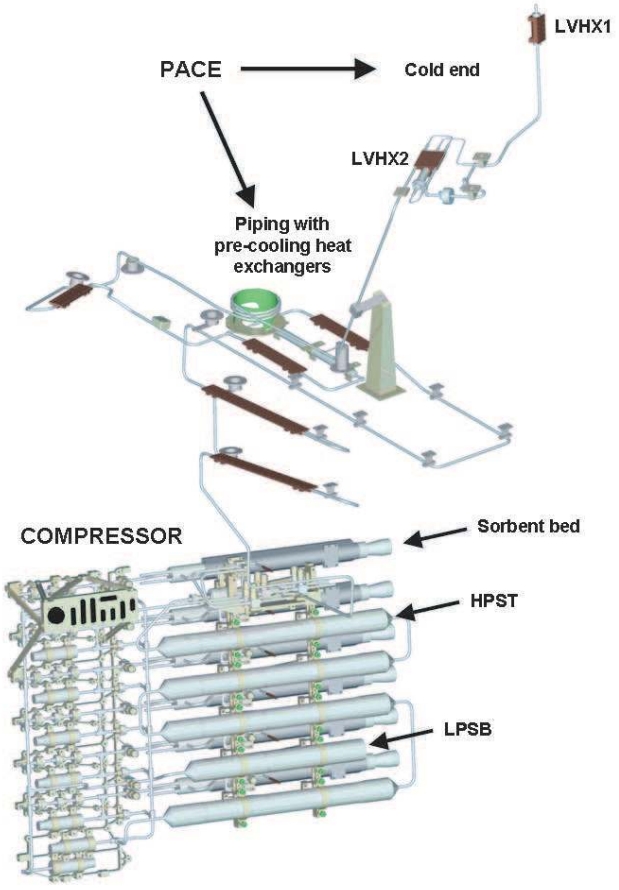

Figure 10. SCS Thermo-Mechanical Unit.

The compressed refrigerant then travels in the Piping and Cold End Assembly (PACE, see Fig. 10), through a series of heat exchangers linked to three V-Groove radiators on the spacecraft which provide passive cooling down to approximately 50 K. Once pre-cooled to the required range of temperatures, the gas is expanded through the J-T valve. Upon expansion, hydrogen forms liquid droplets whose evaporation provides the cooling power. The liquid/vapour mixture then sequentially flows through the two Liquid Vapour Heat eXchangers (LVHX) inside the cold end. LVHX1 and 2 are thermally and mechanically linked to the corresponding instrument (HFI and LFI) interface. The LFI is coupled to the LVHX2 through an intermediate thermal stage, the Temperature Stabilization Assembly (TSA). A feedback control loop (PID type), operated by the cooler electronics, is able to control the TSA peak-to-peak fluctuations down to the required level ($\leq$100 mK). Heat from the instruments evaporates liquid hydrogen and the low pressure gaseous hydrogen is circulated back to the cold sorbent beds for compression.

3.3.3. Performance

The two flight sorption cooler units were delivered to ESA in 2005. Prior to delivery, in early 2004, both flight models underwent sub-system level thermal vacuum test campaigns at JPL. In spring 2006 and summer 2008 respectively, SCS Redundant and Nominal units were tested in cryogenic conditions on the spacecraft FM at the Centre Spatial de Liege (CSL) facilities. Results from these two major test campaigns are summarized in Table 3 and reported in full detail in Morgante et al. (2009b).

4. LFI Programme

The model philosophy adopted for LFI and the SCS was chosen to meet the requirements of the ESA Planck System which assumed from the beginning that there would be three development models of the satellite:

- The Planck Avionics Model (AVM) in which the System Bus was shared with the Herschel satellite, and allowed basic electrical interface testing of all units and communication protocol and software interface verification.
- The Planck Qualification Model (QM) which was limited to the Planck Payload Module (PPLM) containing QMs of LFI, HFI, and the Planck telescope and structure that would allow a qualification vibration test campaign to be performed at payload level, alignment checks, and would, in particular, allow a cryogenic qualification test campaign to be performed on all the advanced instrumentation of the payload that had to fully perform in cryogenic conditions.
- The Planck Protoflight Model (PFM) which contained all the Flight Model (FM) hardware and software that would undergo the PFM environmental test campaign culminating in extended thermal and cryogenic functional performance tests.

4.1. Model Philosophy

In correspondence with the system model philosophy it was decided by the Planck Consortium to follow a conservative incremental approach containing Prototype Demonstrators.

4.1.1. Prototype Demonstrators (PDs)

The scope of the PDs was to validate the LFI radiometer design concept giving early results on intrinsic noise, particularly $1/f$ noise properties, and characterise in a preliminary fashion systematic effects to give requirement inputs for the rest of the instrument design and at satellite level. The PDs also gave the advantage of being able to test and gain experience with very low noise HEMT amplifiers, hybrid couplers, and phase switches.

SCS Unit	Warm Rad T (K)	3 rdVGroove T (K)	Cold End T (K) HFI I/F	Cold End T (K) LFI I/F	Heat Lift (mW)	Input Power (V)	Cycle Time (s)
Redundant	270.5	45	17.2	18.7 [a,b]	1100	297	940
	277	60	18.0	20.1 [a,b]	1100	460	492
	282.6	60	18.4	19.9 [a,b]	1050	388	667
Nominal	270	47	17.1	18.7 [a]	1125	304	940
	273	48	17.5	18.7 [a]	N/A [c]	470	525

[a] Measured at Temperature Stabilization Assembly (TSA) stage
[b] In SCS-Redundant test campaign TSA stage active control was not enabled
[c] Not measured

Table 3. SCS flight units performance summary.

The PD development started early in the programme during the ESA development Pre-Phase B activity and ran in parallel with the successive instrument development phase of elegant bread boarding.

4.1.2. Elegant Breadboarding (EBB)

The fundamental purpose of the LFI EBBs was to demonstrate maturity of the full radiometer design over the whole frequency range of LFI prior to initiating qualification model construction. Thus full comparison radiometers (two channels covering a single polarisation direction) were constructed, centered on 100 GHz, 70 GHz, and 30 GHz, extending from the expected design of the corrugated feed-horns at their entrance to their output stages at their back-end. These were put through functional and performance tests with their front-end sections operating at 20 K as expected in flight. It was towards the end of this development that the financial difficulties which terminated the LFI 100 GHz channel development hit the programme.

4.1.3. The Qualification Model

The development of the LFI QM commenced in parallel with the EBB activities. From the very beginning it was decided that only a limited number of radiometer chain assemblies (RCA), each containing four radiometers (and thus covering fully two orthogonal polarisation directions) at each frequency should be included and that the remaining instrumentation would be represented by thermal mechanical dummies. Thus the LFI QM contained 2 RCA at 70 GHz and one each at 44 GHz and 30 GHz. The active components of the Data Acquisition Electronics (DAE) were thus dimensioned accordingly. The Radiometer Electronics Box Assembly (REBA) QM supplied was a full unit. All units and assemblies went through approved unit level qualification level testing prior to integration as the LFI QM in the facilities of the instrument prime contractor Thales Alenia Space Milano.

The financial difficulties that have already been mentioned also disrupted QM development and lead to the use by ESA of a thermal-mechanical representative dummy of LFI in the system level satellite QM test campaign because of the ensuing delay in the availability of the LFI QM. The LFI QM was however fundamental in the development of LFI as it gave the LFI Consortium the opportunity to perform representative cryo-testing of a reduced model of the instrument and thus confirm the design of the LFI flight Model.

4.1.4. The Flight Model

The LFI FM contained flight standard units and assemblies that went through flight unit acceptance level tests prior to integration as the LFI FM. In addition prior to mounting in the LFI FM each RCA went through a separate cryogenic test campaign after assembly to allow preliminary tuning to achieve best performance and confirm the overall functional performance of each radiometer. At the LFI FM test level the instrument went through an extended cryogenic test campaign that included a further level of tuning and the instrument calibration that could not be performed when mounted in the final configuration on the satellite because of schedule and cost constraints. At the time of delivery of the LFI FM to ESA for integration on the satellite the only significant verification test that remained to be done was the vibration testing of the fully assembled Radiometer Array Assembly (RAA) that could not be done in a meaning-full way at instrument level because of the problem of simulating the coupled vibration input through the DAE and the LFI FPU mounting in to the RAA (and in particular in to the waveguides). This verification was completed successfully during the satellite PFM vibration test campaign.

4.1.5. The Avionics Model

The LFI AVM was composed of the DAE QM, and its secondary power supply box removed from the RAA of the LFI QM, an AVM model of the REBA and the QM instrument harness. No radiometers were present in the LFI AVM, and their active inputs on the DAE were terminated with resistors. The LFI AVM was used successfully by ESA in the Planck System AVM test campaigns to fulfil its scope outlined above.

4.2. The Sorption Cooler Sub-system Model Philosophy

The SCS model development was designed to produce two coolers - a nominal cooler and a redundant cooler. The early part of the model philosophy adopted was similar to that of LFI employing prototype development and testing of key components such as single compressor beds prior to the building of an EBB containing a complete complement of components as in a cooler intended to fly. This EBB cooler was submitted to an intensive functional and performance test campaign. The Sorption Cooler Electronics (SCE) meanwhile started development with an EBB and was followed by a QM and then FM1/FM2 build.

The TMUs of both the nominal and redundant sorption coolers went through protoflight unit testing prior to assembly with their respective PACE for thermal/cryogenic testing before delivery. To conclude the qualification of the PACE a spare unit

participated in the PPLM QM system level vibration and cryogenic test campaign.

An important constraint in the ground operation of the sorption coolers is that they could not be fully operated with their compressor beds far from a horizontal position. This was to avoid permanent non homogeneity in the distribution of the hydrides in the compressor beds and the ensuing loss in efficiency. In the fully integrated configuration of the satellite, the PFM thermal and cryogenic test campaign, for test chamber configuration, schedule and cost reasons would allow only one cooler to be in a fully operable orientation. Thus the first cooler to be supplied, which was designated the redundant cooler (FM1), was mounted with the PPLM QM and put through a cryogenic test campaign (termed PFM1) with similar characteristics to those of the final thermal balance and cryogenic tests of the fully integrated satellite. Then FM1 was later integrated into the satellite where only short, fully powered, health checking was done on it. The second cooler was designated as the nominal cooler (FM2) and participated fully in the final cryo-testing of the satellite. For both coolers final verification (TMU assembled with PACE) was achieved during the Planck system level vibration test campaign and subsequent tests.

The AVM of the SCS was supplied using the QM of the SCE and a simulator of the TMU to simulate the power load of a real cooler.

4.3. System Level Integration and Test

The Planck satellite together with the instruments was integrated in the Thales Alenia Space facilities at Cannes in France.

The SCS nominal and redundant coolers were integrated on to the Planck satellite before LFI and HFI.

Prior to integration on the satellite, the HFI FPU was integrated in to the FPU of LFI. This involved mounting the LFI 4K-Loads on HFI before starting the main integration process which was a very delicate operation considering that when done the closest approach of LFI and HFI would be of the order of 2 mm. It should be remembered that LFI and HFI had not "met" during the Planck QM activity and so this integration was performed for the first time during the Planck PFM campaign. The integration process had undergone much study and required a special rotatable GSE for the LFI RAA, and a special suspension and balancing system to allow HFI to be lifted and lowered in to LFI at the correct orientation along guide rails from above. Fortunately the integration was completed successfully.

Subsequently the combined LFI RAA and HFI FPU were integrated on to the satellite supported by the LFI GSE which was eventually removed during integration to the telescope. The process of electrical integration and checkout was then completed for LFI, the SCS and HFI, and the Proto-Flight Model test campaign was commenced.

For LFI this test campaign proceeded with ambient functional checkout followed by detailed tests as a complete subsystem prior to participation with the SCS and HFI in the sequence of alignment, EMC, sine and random acoustic vibration tests, and the sequence of system level verification tests with the Mission Operations Control Centre (MOC at ESOC, Darmstadt) and LFI DPC. During all these tests, at key points, both the nominal and redundant SCS were put through ambient temperature health checks to verify basic functionality.

The environmental test campaign culminated with the thermal balance and cryogenic tests carried out in the Focal 5 facility of the Centre Spatial de Liege, Belgium. The test was designed to follow very closely the expected cool-down scenario after launch through to normal mission operations and it was during these tests that the two instruments and the Sorption Cooler directly demonstrated together not only their combined capabilities but also their operational margins, with success.

5. LFI test and verification

The LFI has been tested and calibrated before launch at various levels of integration, from the single components up to instrument and satellite levels; this approach, which is summarised schematically in Fig. 11, provided inherent redundancy and optimal instrument knowledge.

Passive components, i.e. feed-horns, OMTs and waveguides, have been tested at room conditions at the Plasma Physics Institute of the National Research Council (IFP-CNR) using a Vector Network Analyser. A summary of the measured performance parameters is provided in Table 4; measurements and results are discussed in detail in Villa et al. (2009a); D'Arcangelo et al. (2009b,a).

Table 4. Measured performance parameters of the LFI passive components.

Feed Horns	Return Loss [1], Cross-polar (±45°) and Co-polar patterns (E, H and ±45° planes) in amplitude and phase, Edge taper at 22°
OMTs	Insertion Loss, Return Loss, Cross-polarisation, Isolation
Waveguides	Insertion Loss, Return Loss, Isolation

[1] return loss and patterns (E,H for all frequencies, also ±45 and cross-polar for the 70GHz system) have been measured for the assembly FH+OMT as well.

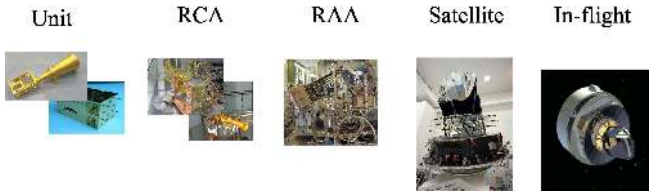

Figure 11. Schematic of the various calibrations steps in the LFI development.

Also radiometric performance was measured several times during the LFI development on individual sub-units (amplifiers, phase switches, detector diodes, etc.) on integrated front-end and back-end modules (Davis et al. 2009; Artal et al. 2009; Varis et al. 2009) and on the complete radiometric assemblies both as independent RCAs (Villa et al. 2009b) and in RAA, the final integrated instrument configuration (Mennella et al. 2009).

In Table 5 (taken from Mennella et al. (2009)) we list the main LFI radiometric performance parameters and the integration levels at which they have been measured. After the flight instrument test campaign the LFI has been cryogenically tested again after integration on the satellite with the HFI while the final characterisation will be performed in flight before starting nominal operations.

RCA and RAA test campaigns have been key to characterise the instrument functionality and behaviour, and measure its ex-

Table 5. Main calibration parameters and where they have been / will be measured. The following abbreviations have been used: SAT = Satellite, FLI = In-flight, FE = Front-end, BE = Back-end, LNA = Low Noise Amplifier, PS = Phase Switch, Radiom = Radiometric, Susc = Susceptibility.

Category	Parameters	RCA	RAA	SAT	FLI
Tuning	FE LNAs	Y	Y	Y	Y
	FE PS	Y	Y	Y	Y
	BE offset and gain	Y	Y	Y	Y
	Quantisation / compression	N	Y	Y	Y
Radiom.	Photometric calibration	Y	Y	Y	Y
	Linearity	Y	Y	Y	Y
	Isolation	Y	Y	Y	Y
	In-band response	Y	N	N	N
Noise	White noise	Y	Y	Y	Y
	Knee freq.	Y	Y	Y	Y
	$1/f$ slope	Y	Y	Y	Y
Susc.	FE temperature fluctuations	Y	Y	Y	Y
	BE temperature fluctuations	Y	Y	N	N
	FE bias fluctuations	Y	Y	N	N

pected performance in flight conditions. In particular 30 GHz and 44 GHz RCAs have been integrated and tested in Italy, at the Thales Alenia Space (TAS-I) laboratories in Milan, while the 70 GHz RCA test campaign has been carried out in Finland at the Yilinen-Elektrobit laboratories (Villa et al. 2009b). After this testing phase the 11 RCAs have been collected and integrated with the flight electronics in the LFI main frame at the TAS-I labs where the instrument final test and calibration has taken place (Mennella et al. 2009). Custom-designed cryofacilities (Terenzi et al. 2009b; Morgante et al. 2009a) and high-performance black-body input loads (Terenzi et al. 2009a; Cuttaia et al. 2009) have been developed in order to test the LFI in the most flight-representative environmental conditions.

A particular point must be made about the front-end bias tuning which is a key step in setting the instrument scientific performance. Tight mass and power constraints called for a simple design of the DAE box so that power bias lines have been divided in five common-grounded power groups with no bias voltage readouts. Only the total drain current flowing through the front-end amplifiers is measured and is available in the housekeeping telemetry.

This design has important implications on front-end bias tuning, which depends critically on the satellite electrical and thermal configuration. Therefore this step has been repeated at all integration stages and will also be repeated during ground satellite tests and in flight before the start of nominal operations. Details about bias tuning performed on front-end modules and on the individual integrated RCAs can be found in Davis et al. (2009), Varis et al. (2009) and Villa et al. (2009b).

Parameters measured on the integrated instrument have been found essentially in line with measurements performed on individual receivers; in particular the LFI shows excellent $1/f$ stability and rejection of instrumental systematic effects. On the other hand the very ambitious sensitivity goals have not been fully met and the white noise sensitivity (see Table 6) is ∼30% higher than requirements. Nevertheless, the measured performance makes LFI the most sensitive instrument of its kind, a factor of 2 to 3 better than WMAP [8] at the same frequencies.

Table 6. Calibrated white noise from ground test results extrapolated at CMB input signal level. Two different methods are used here to provide a reliable range of values (see Mennella et al. (2009) for further details). The final verification of sensitivity will be derived in flight during the CPV phase.

Frequency channel	30GHz	44GHz	70GHz
White noise per ν channel $[\mu\mathrm{K}\cdot\sqrt{\mathrm{s}}]$	141÷154	152÷160	130÷146

6. LFI Data Processing Centre

In order to take maximum advantage of the capabilities of the Planck mission and to achieve its very ambitious scientific objectives, proper data reduction and scientific analysis procedures were defined, designed, and implemented very carefully. The data processing was optimized so as to extract the maximum amount of useful scientific information from the data set and to deliver the calibrated data to the broad scientific community within a rather short period of time. As demonstrated by many previous space missions using state-of-the-art technologies, the best scientific exploitation is obtained by combining the robust, well-defined architecture of a data pipeline and its associated tools with the high scientific creativity essential when facing unpredictable features of the real data. Although many steps required for the transformation of data have been defined during the development of the pipeline, since most of the foreseeable ones have been implemented and tested during simulations, some of them will remain unknown until flight data are obtained.

Planck is a PI mission, and its scientific achievements will depend critically on the performance of the two instruments, LFI and HFI, on the cooling chain, and on the telescope. The data processing will be performed by two Data Processing Centres (DPCs) (Pasian et al. 2000; Pasian & Gispert 2000; Pasian & Sygnet 2002). However, despite the existence of two separate distributed DPCs, the success of the mission relies heavily on the combination of the measurements from both instruments.

The development of the LFI DPC software has been performed in a collaborative way across a consortium spread across over 20 institutes in a dozen countries. Individual scientists belonging to the Software Prototyping Team develop prototype code, which is then delivered to the LFI DPC Integration Team. The latter is responsible for integrating, optimizing and testing the code, and has produced the pipeline software to be used during operations. This development takes advantage of tools defined within the Planck IDIS (Integrated Data and Information System) collaboration.

A software policy has been defined, with the aim of allowing the DPC to run the best possible algorithms within its pipeline, while fostering collaboration inside the LFI Consortium and across Planck, and preserving at the same time the intellectual property of the code authors on the processing algorithms devised.

The Planck DPCs are responsible for the delivery and archiving of the following scientific data products, which are the deliverables of the Planck mission:

[8] Calculated on the final resolution element per unit integration time.

– Calibrated time series data, for each receiver, after removal of systematic features and attitude reconstruction.
– Photometrically and astrometrically calibrated maps of the sky in each of the observed bands.
– Sky maps of the main astrophysical components.
– Catalogues of sources detected in the sky maps of the main astrophysical components.
– CMB Power Spectrum coefficients and a likelihood code.

Additional products, necessary to the total understanding of the instrument, are being negotiated for inclusion in the Planck Legacy Archive (PLA). The products foreseen to be added to the formally defined products mentioned above are:

– Data sets defining the estimated characteristics of each detector and the telescope (e.g. detectivity, emissivity, time response, main beam and side lobes, etc. ...).
– "Internal" data (e.g. calibration data sets, data at intermediate level of processing);
– Ground Calibration and AIV Databases produced during the instrument development; and gathering all information, data and documents relative to the overall payload and all systems and sub-systems. Most of this information is crucial for processing flight data and updating the knowledge and the performance of the instrument.

The LFI DPC processing can be logically divided in three levels:

– Level 1: includes monitoring of instrument health and behaviour and the definition of corrective actions in the case of unsatisfactory functioning, and the generation of Time Ordered Information (TOI), a set of ordered information on a temporal basis or scan-phase basis, as well as data display, checking and analysis tools.
– Level 2: TOIs produced at Level 1 will be cleaned up by taking away noise and many other types of systematic effects on the basis of calibration information. The final product of the Level 2 includes "frequency maps".
– Level 3: "Component maps" will be generated by this level through a decomposition of individual "frequency maps" using also products from the other instrument and, possibly, ancillary data.

One additional level (Level S) is used to develop the most sophisticated simulations based on actual instrument parameters extracted during the ground test campaigns, was also implemented.

We describe in the following sections the DPC Levels and the software infrastructure, and we finally report briefly on the tests that were applied to ensure that all pipelines are ready for the launch.

6.1. DPC Level 1

Level 1 takes input from the MOC's (Mission Operation Centre) Data Distribution System (DDS), decompresses the raw data, and outputs Time Ordered Information for Level 2. Level 1 does not include scientific processing of the data; actions are performed automatically by using pre-defined input data and information from the technical teams. The input to Level 1 are telemetry (TM) and auxiliary data as they are released by the MOC. Level 1 uses TM data for performing a routine analysis (RTA - Real Time Assessment) of the Spacecraft and Instrument status, in addition to what is performed at the MOC, with the aim of monitoring the overall health of the payload and detecting possible anomalies. A quick-look data analysis (TQL - Telemetry Quick Look) of the science TM is also done, to monitor the operation of the observation plan and to verify the performance of the instrument. The processing is meant to lead to the full mission raw-data stream in a form suitable for subsequent data processing by the DPC.

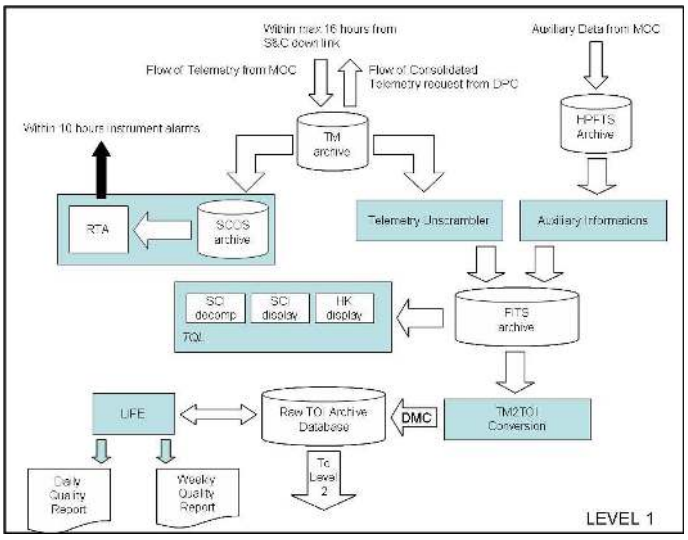

Figure 12. Level 1 structure.

Level 1 deals also with all activities related to the production of reports. This task includes the results of telemetry analysis, but also the results of technical processing carried out on Time-Ordered Information (TOI) to understand the current and foreseen behaviour of the instrument. This second item includes specific analysis of instrument performance (LIFE - LFI Integrated perFormance Evaluator), and more general checking of time series (TSA - Time Series Analysis) for trend analysis purposes and comparison with the TOI from the other instrument. Additional tasks of Level 1 relate to its role of instrument control and DPC interface with the MOC. In particular, the following actions are performed:

– Preparation of telecommanding procedures aimed at modifying the instrument setup.
– Preparation of instrument database (MIBs).
– Communicate to the MOC "longer-term" inputs deriving from feedback from DPC processing.
– Calibration of REBA parameters to fit long term trends in the instrument setup.

In Level 1 all actions are planned to be performed on a "day-to-day" basis during observation. In Fig. 12 the structure of Level 1 and time required is reported. For more details refer to (Zacchei et al. 2009).

6.2. DPC Level 2

At this level data processing steps requiring detailed instrument knowledge (data reduction proper) will be performed. The raw time series from Level 1 will be also used for reconstructing a number of sets of calibrated scans per each detector, as well as instrumental performance and properties, and maps of the sky for each channel. The processing is iterative, since simultaneous evaluation of quite a number of parameters should be made before the astrophysical signal can be isolated and averaged over all detectors in each frequency channel. Continuous exchange of information between the two DPCs, will be necessary at Level 2

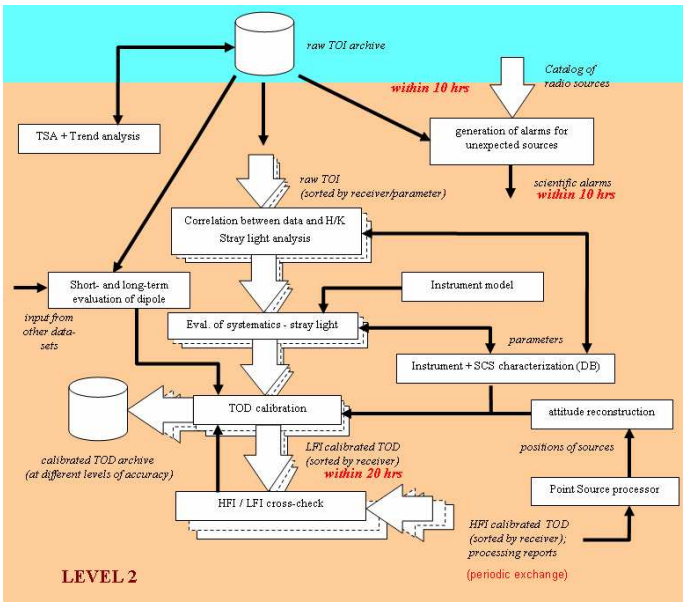

Figure 13. Level 2 Calibration pipeline.

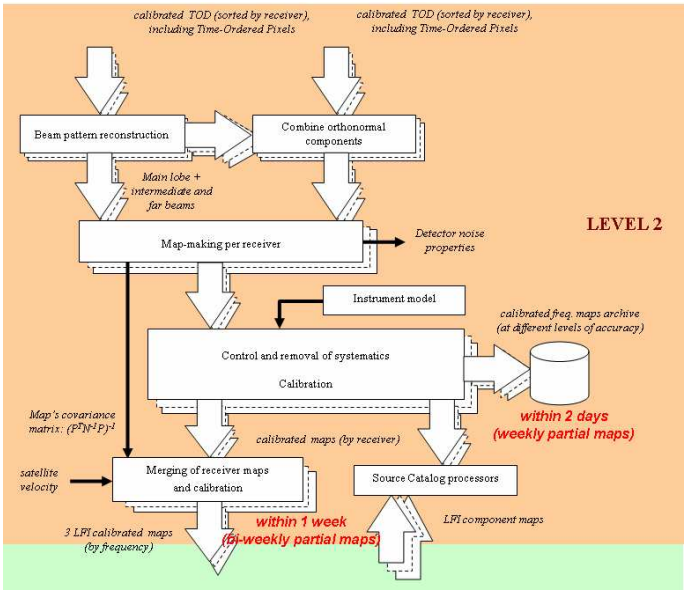

Figure 14. Level 2 MapMaking pipeline.

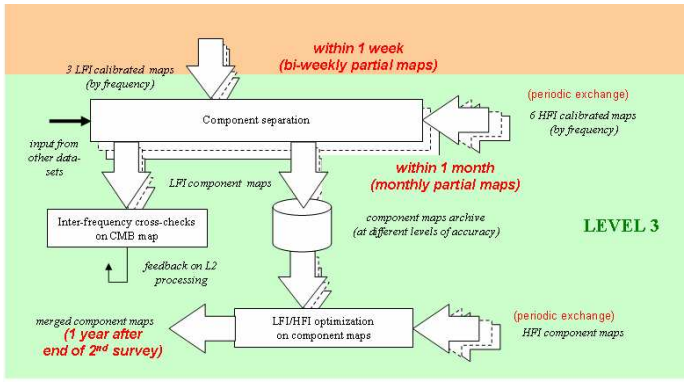

Figure 15. Level 3 pipeline structure.

in order to identify any suspect or unidentified behaviour or any results from the detectors.

The first task that the Level 2 performs is the creation of differenced data. Level 1 stores data from both Sky and Load. These two have to be properly combined to produce differenced data therefore reducing the impact of 1/f noise. This is done via the computation of the so-called gain modulation factor "R" which is derived taking the ratio of the mean signals from both Sky and Load.

After differenced data are produced, the next step is the photometric calibration which transforms the digital unit in physical units. This operation is quite complex: different methods are implemented in the Level 2 pipeline that use the CMB dipole as an absolute calibrator allowing to convert data into physical units.

Another major task is beam reconstruction, which is implemented using information from planet crossings. We developed an algorithm performing a bi-variate approximation of the main beam section of the antenna pattern and reconstructing the position of the horn in the focal plane and its orientation with respect to a reference axis.

The step following the production of calibrated timelines is the creation of calibrated frequency maps. In order to do this, pointing information will be encoded into Time-Ordered Pixels i.e. pixel numbers in the given pixelisation scheme (HEALPix) identifying a given pointing direction ordered in time. In order to produce temperature maps it is necessary to reconstruct the beam pattern for the two polarization directions for the main, intermediate and far part of the beam pattern. This will allow combination of the two orthogonal components into a single temperature timeline. On this temperature timeline a map-making algorithm will be applied to produce a map from each receiver.

The instrument model allows one to check and control systematic effects, and the quality of the removal performed by map-making and calibration of the receiver map. Receiver maps cleaned from systematic effects at different levels of accuracy will be stored into a calibrated maps archive. The production of frequency calibrated maps is done processing together all receivers from a given frequency channel in a single map-making run. In Figures 13 and 14 we report the steps performed by the Level 2 with the foreseen time associated.

6.3. DPC Level 3

The goal of the DPC Level 3 is to estimate and characterise maps of all the different astrophysical and cosmological sources of emission ("components") present at Planck wavelengths. Using the CMB component obtained after point source extraction and cleaning from diffuse, Galactic emission, the angular power spectrum of the CMB is estimated for temperature, polarisation and cross temperature/polarisation modes.

The extraction of the signal coming from Galactic point-like objects, other Galaxies and clusters of them is achieved as a first step, either using pre-existing catalogues based on non-Planck data, and filtering the multi-frequency maps with optimal filters for the detection and identification of beam like objects (see Herranz et al. (2009) and references therein).

The algorithms dedicated to the separation of diffuse emissions fall into to four main categories, depending on the criteria exploited to achieve separation, and making use of the wide frequency coverage of Planck (see Leach et al. (2008) and references therein). Internal Linear Combination and Template Fitting achieve linear mixing and combination of the multi-frequency data with other datasets, optimized for CMB or foreground recovery. The Independent Component Analysis works in the statistical domain, without making use of foreground modeling or spatial correlations in the data, but assuming instead sta-

tistical independence between the components to recover. The correlated component analysis, on the other hand, makes use of a parametrization of foreground unknowns, and uses spatial correlations in order to achieve separation. Finally, Parametric Methods consist in modeling foreground and CMB treating each resolution element independently, achieving fitting of the unknowns and separation by means of a maximum likelihood analysis. The LFI DPC Level3 includes algorithms belonging to each of the four categories outlined above. The complementarity of different methods for different purposes, as well as the cross check on common products, are required for achieving reliable and complete scientific products.

As for power spectrum estimation, two independent and complementary approaches have been implemented (see Gruppuso et al. (2009), and references therein): a Monte-Carlo method suitable for high multipoles (based on the MASTER approach but including cross-power spectra from independent receivers) and a maximum-likelihood method for low multipoles. A combination of the two methods will be used to produce the final estimation of the angular power spectrum from LFI data, before combining with HFI data. In Fig. 15 we report the steps performed in the the Level 3 pipeline with the foreseen timescale associated.

The inputs to the Level 3 pipeline are the three calibrated frequency maps from LFI together with the six calibrated HFI frequency maps that are planned to be exchanged on a monthly basis. The Level 3 pipeline has links with most of the stages of Level 1 and Level 2 pipelines, and therefore the most complete and detailed knowledge of the instrumental behavior is most important for achiveing its goals. Systematic effects appearing in the time ordered data, beam shapes, band width, source catalogues, noise distribution and statistics are examples of important inputs to the Level 3 processing. Level 3 will produce source catalogues, component maps and CMB power spectra that will be delivered to the Planck Legacy Archive (PLA) together with other information and data needed for the public release of the Planck products.

6.4. DPC Level S

It was widely agreed within both Consortia that a software able to simulate the instrument footprint, starting from a predefined sky, was indispensable for the full period of the Planck mission. Based on that idea, an additional processing level, Level S, was developed, and was upgraded whenever the knowledge of the instrument improved (Reinecke et al. 2006). Level S includes now all the instrument characteristics as they were understood during the ground test campaign. Simulated data were used to evaluate the performance of data-analysis algorithms and software vs the scientific requirements of the mission and to demonstrate the capability of the DPCs to work using blind simulations that contain unknown parameter values to be recovered by the data processing pipeline.

6.5. DPC Software Infrastructure

During the whole of the Planck project it was, and it will be, necessary to deal with aspects related to information management, which pertain to a variety of activities concerning the whole project, ranging from instrument information (technical characteristics, reports, configuration control documents, drawings, public communications, etc.), to software development/control (including the tracking of each bit produced by each pipeline).

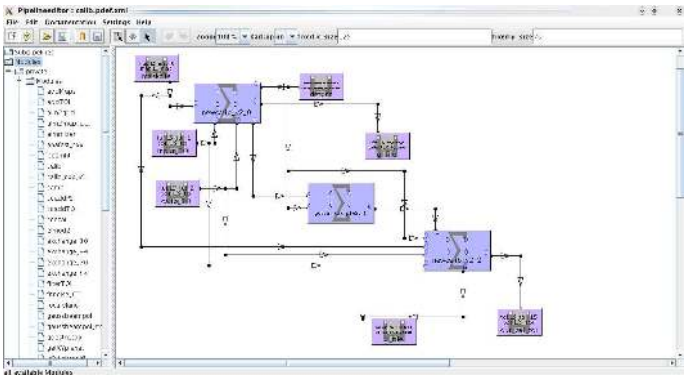

Figure 16. IDIS ProC pipeline Editor.

For this purpose, an Integrated Data and Information System (IDIS) was developed. IDIS (Bennett et al. 2000) is a collection of infrastructure software for supporting the Planck Data Processing Centres in their management of large quantities of software, data and ancillary information. The infrastructure is relevant to the development, operational and post-operational phases of the mission.

The full IDIS can be broken down into five major components:

- Document Management System (DMS), to store and share documents
- Data Management Component (DMC), allowing the ingestion, efficient management and extraction of the data (or subsets thereof) produced by Planck activities.
- Software Component (SWC), allowing to administer, document, handle and keep under configuration control the software developed within the Planck project.
- Process Coordinator (ProC), allowing the creation and run of processing pipelines inside a predefined and well controlled environment.
- Federation Layer (FL), which allows controlled access to the previous objects and acts as a glue between them.

The use of the DMS allowed the entire consortia to ingest and store hundreds of documents with an efficient way to retrieve them. The DMC is an API (Application Programming Interface) for data input/output, connected to a database (either relational or object oriented) and aimed at archiving and retrieval of data and the relevant meta-information; it also features a user GUI. The ProC is a controlled environment in which software modules can be added to create an entirely functional pipeline. It stores all the information related to versioning of the modules used, data, temporary data created within the database while using the DMC API. In Fig. 16 an example of LFI pipeline is shown. Finally, the FL is an API that, using a remote LDAP database, assigns the appropriate permission to the users with reference to data access, software access and pipeline run privileges.

6.6. DPC Test performed

Each pipeline and sub-pipeline (Level 1, Level 2 and Level 3) have undergone different kinds of tests. We report here only the official tests conducted with ESA, without referring to the internal tests which were dedicated to DPC subsystems. Level 1 was the most heavily tested as this pipeline is considered launch-critical. As a first step it was necessary to validate the output with respect to the input: to do that we ingested in the instrument a well known signal as described in (Frailis et al.

2009) with the purpose of verifying if the processing inside Level 1 was correct. This had also the benefit to give an independent test of important functionalities for the REBA software responsible for the onboard preprocessing of scientific data. Afterwards more complete tests, including all interfaces with other elements of the ground segment, were performed. Those tests simulate one week of nominal operations (SOVT1 - System Operation Validation Test) (Keck 2008) and, during the SOVT2, one week of Commissioning Performance Verification (CPV) phase. During these tests we demonstrated that the LFI Level 1 is able to deal with the telemetry as it should be acquired during operations.

Tests performed on Level 2 and Level 3 were more science oriented to demonstrate the scientific adequacy of the LFI DPC pipeline, i.e. its ability to produce scientific results commensurate to the objectives of the Planck mission. These tests were based on blind simulations of growing complexity. The Phase 1 test data, produced with Level S, featured some simplifying approximations:

- the sky model was based on the "concordance model" CMB (no non-gaussianity);
- the dipole did not include modulations due to the Lissajous orbit around L2;
- Galactic emission was obtained assuming non-spatially varying spectral index;
- the detector model was "ideal" and did not vary with time;
- the scanning strategy was "ideal" (i.e. no gaps in the data).

The results of this test were in line with the objective of the mission (see Perrotta & Maino (2007)).

The Phase 2 tests are still ongoing. They take into account more realistic simulations with all the known systematics and known problems (e.g. data gaps) in the data. Results are expected in May 2009.

7. Conclusion

Ground testing shows the LFI works as anticipated. The observational program will start after the Planck/Herschel launch on May 14th, 2009.

A challenging commissioning and final calibration phase will prepare the LFI for nominal operations that will start about 90 days after launch. After ~20 days the instrument will be switched on and its functionality will be tested in parallel with the cool down of the 20 K stage. Then the cool down period of the HFI focal plane down to 4 K will be exploited by the LFI to tune voltage biases of the front end amplifiers, phase switches, and REBA parameters, which will set the final scientific performance of the instrument. Final tunings and calibration will be performed in parallel with HFI activities for about 25 days until the last in-flight calibration phase (the so-called "first light survey"), 14 days of data acquisition in nominal mode that will benchmark the whole system, from satellite and instruments to data transmission, ground segment and data processing levels.

The first light survey will produce the very first Planck maps. This will not be aimed to scientific exploitation but will rather serve as a final test of the instrumental and data processing capabilities of the mission. After this, the Planck scientific operations will begin.

8. Acknowledgements

Planck is a project of the European Space Agency with instruments funded by ESA member states, and with special contributions from Denmark and NASA (USA). The Planck-LFI project is developed by an International Consortium led by Italy and involving Canada, Finland, Germany, Norway, Spain, Switzerland, UK, USA. The Italian contribution to Planck is supported by the Italian Space Agency (ASI) and INAF. We wish also to thank the many people of the Herschel/Planck Project and RSSD of ESA, ASI, THALES Alenia Space Industries and the LFI Consortium that have contributed to the realization of LFI. We are grateful to our HFI colleagues for such a fruitful collaboration during so many years of common work. The German participation at the Max-Planck-Institut für Astrophysik is funded by the Bundesministerium für Wirtschaft und Technologie through the Raumfahrt-Agentur of the Deutsches Zentrum für Luft- und Raumfahrt (DLR) [FKZ: 50 OP 0901] and by the Max-Planck-Gesellschaft (MPG). The Finnish contribution is supported by the Finnish Funding Agency for Technology and Innovation (Tekes) and the Academy of Finland. The Spanish participation is funded by Ministerio de Ciencia e Innovacion through the project ESP2004-07067-C03 and AYA2007-68058-C03. C. Baccigalupi and F. Perrotta acknowledge partial support of the NASA LTSA Grant NNG04CG90G. We acknowledge the use of the BCX cluster at CINECA under the agreement INAF/CINECA. We acknowledge the use of the Legacy Archive for Microwave Background Data Analysis (LAMBDA). Support for LAMBDA is provided by the NASA Office of Space Science. We acknowledge use of the HEALPix (Górski et al. 2005) software and analysis package for deriving the results in this paper.

Appendix A: List of Acronyms

ADAF/ADIOS = Advection Dominated Accretion Flow/ Advection Dominated In-flow Out-flow Solution
AIV = Assembly Integration and Verification
API = Application Programming Interface
APS = Angular Power Spectrum
ASI = Agenzia Spaziale Italiana (Italian Space Agency)
ATCA = Australian Telescope Compact Array
AVM = AVionic Model
BEM = Back-End Module
BEU = Back-End Unit
C-BASS = C-Band All-Sky Survey
CDM = Cold Dark Matter
COBE = COsmic Background Explorer
COBRAS = COsmic Background Radiation Anisotropy Satellite
CMB = Cosmic Microwave Background
CSL = Centre Spatial de Liege
DAE = Data Acquisition Electronics
DBI = Dirac-Born-Infeld (inflation)
DC = Direct Current
DDS = Data Distribution System
DMC = Document Management Component
DMS = Document Management System
DPC = Data Processing Centre
EBB = Elegant BreadBoarding
ESA = European Space Agency
ET = Edge Taper
FEM = Front-End Module
FL = Federation Layer
FM = Flight Model
FSRQ = Flat Spectrum Radio Quasar

FWHM = Full Width Half Maximum
GEM = Galactic Emission Mapping
GLAST = Gamma ray Large Area Space Telescope
GLS = Generalized Least Square
GSE = Grand Support Equipment
GUI = Graphical User Interface
HEALPix = Hierarchical Equal Area isoLatitude Pixelization
HEMT = High Electron Mobility Transistor
HFI = High Frequency Instrument
HPST = High-Pressure Stabilization Tank
ICA = Independent Component Analysis
IDIS = Integrated Data and Information System
ILC = Internal Linear Combination
IR = Infra Red
ISM = Inter Stellar Medium
LBSP = Low-Pressure Storage Bed
LDAP = Lightweight Directory Access Protocol
LFI = Low Frequency Instrument
LIFE = LFI Integrated perFormance Evaluator
LNA = Low Noise Amplifier
LVHX = Liquid Vapour Heat eXchange
MIB = Mission Information Base
MIC = Microwave Integrated Circuit
MMIC = Monolothic Microwave Integrated Circuit
MOC = Mission Operation Centre
NG = Non Gaussianity
OMT = Orthomode Transducer
PACE = Piping and Cold End Assembly
PD = Prototype Demonstrator
PFM = Planck Prototype Model
PGMS = Parkes Galactic Meridian Survey
PI = Principal Investigator
PID = Proportional Integral Derivative
PILOT = Polarized Instrument for the Long wavelength Observations of the Tenuous ISM
PLA = Planck Legacy Archive
PPLM = Planck PayLoad Module
ProC = Process Coordinator
PS =Phase Switch
QM = Qualification Model
QUIJOTE = Q U I JOint TEnerife
RAA = Radiometer Array Assembly
RCA = Radiometer Chain Assembly
REBA = Radiometer Electronics Box Assembly
RF = Radio Frequency
RTA = Real Time Assessment
SAMBA = SAtellite for Measurements of Background Anisotropies
SCE = Sorption Cooler Electronics
SCS = Sorption Cooler Sub system
SS = Scanning Strategy
SVM = Service Module
SWC = SoftWare Component
TM = TeleMetry
TMU = Thermo-Mechanical Unit
TOI = Time Order Information
TQL = Telemetry Quick Look
TSA = Temperature Stabilization Assembly
WMAP = Wilkinson Microwave Anisotropy Probe
WR = Warm Radiator
XPD = Cross Polar Discrimination

References

Aatrokoski, J., Lähteenmäki, A., Tornikoski, M., et al. 2009, submitted to MNRAS
Abdo, A. A. 2009, ArXiv e-prints 0902.1559
Abramo, L. R., Bernui, A., Ferreira, I. S., Villela, T., & Wuensche, C. A. 2006, Phys. Rev. D, 74, 063506
Artal, E., Aja, B., L. de la Fuente, M., et al. 2009, J. Inst., submitted, (companion paper)
Ashdown, M. A. J., Baccigalupi, C., Balbi, A., et al. 2007, A&A, 467, 761
Ashdown, M. A. J., Baccigalupi, C., Bartlett, J. G., et al. 2009, A&A, 493, 753
Babich, D. & Zaldarriaga, M. 2004, Phys. Rev. D, 70, 083005
Barbosa, D., Bergano, J., Fonseca, R., et al. 2006, in PoS(CMB2006)029, CMB and Physics of the Early Universe, ed. G. de Zotti, et al.
Bartlett, J. G., Chamballu, A., Melin, J.-B., Arnaud, M., & Members of the Planck Working Group 5. 2008, Astronomische Nachrichten, 329, 147
Bartolo, N., Komatsu, E., Matarrese, S., & Riotto, A. 2004, Phys. Rep., 402, 103
Bartolo, N. & Riotto, A. 2009, Journal of Cosmology and Astro-Particle Physics, 3, 17
Bennett, K., Pasian, F., Sygnet, J.-F., et al. 2000, in Society of Photo-Optical Instrumentation Engineers (SPIE) Conference Series, Vol. 4011, Society of Photo-Optical Instrumentation Engineers (SPIE) Conference Series, ed. R. I. Kibrick & A. Wallander, 2–10
Bernard, J.-P., Ade, P., de Bernardis, P., et al. 2007, in EAS Publications Series, Vol. 23, EAS Publications Series, ed. M.-A. Miville-Deschênes & F. Boulanger, 189–203
Bersanelli, M., Mandolesi, N., Butler, R., et al. 2009, A&A, submitted, (companion paper)
Bersanelli, M., Mattaini, E., Santambrogio, E., et al. 1998, Experimental Astronomy, 8, 231
Bhandari, P., Prina, M., Bowman, J., et al. 2004, Advances in Cryogenic Engineering, 44, 395
Bonaldi, A., Ricciardi, S., Leach, S., et al. 2007, MNRAS, 382, 1791
Burigana, C., La Porta, L., Reich, W., et al. 2006, in PoS(CMB2006)016, CMB and Physics of the Early Universe, ed. G. de Zotti, et al.
Burigana, C., Malaspina, M., Mandolesi, N., et al. 1997, A preliminary study on destriping techniques of PLANCK/LFI measurements versus observational strategy, Tech. Rep. 198/1997, TeSRE/CNR - Bologna, arXiv:astro-ph/9906360
Burigana, C., Natoli, P., Vittorio, N., Mandolesi, N., & Bersanelli, M. 2001, Experimental Astronomy, 12, 87
Burigana, C., Sandri, M., Villa, F., et al. 2004, A&A, 428, 311
Cho, J. & Lazarian, A. 2003, New Astronomy Review, 47, 1143
Collaudin, B. & Passvogel, T. 1999, Cryogenics, 39, 157
Copi, C. J., Huterer, D., Schwarz, D. J., & Starkman, G. D. 2007, Phys. Rev. D, 75, 023507
Copi, C. J., Huterer, D., Schwarz, D. J., & Starkman, G. D. 2008, ArXiv e-prints 0808.3767
Copi, C. J., Huterer, D., & Starkman, G. D. 2004, Phys. Rev. D, 70, 043515
Cremonese, G., Marzari, F., Burigana, C., & Maris, M. 2002, New Astronomy, 7, 483
Cruz, M., Martínez-González, E., Vielva, P., & Cayón, L. 2005, MNRAS, 356, 29
Cumberbatch, D. T., Zuntz, J., Kamfjord Eriksen, H. K., & Silk, J. 2009, ArXiv e-prints 0902.0039
Cuttaia, F., Bersanelli, M., Battaglia, P., et al. 2009, J. Inst., submitted, (companion paper)
Dallacasa, D., Stanghellini, C., Centonza, M., & Fanti, R. 2000, A&A, 363, 887
D'Arcangelo, O., Figini, L., Simonetto, A., et al. 2009a, J. Inst., submitted, (companion paper)
D'Arcangelo, O., Simonetto, A., Figini, L., et al. 2009b, J. Inst. submitted, (companion paper)
Davis, R., Wilkinson, A., Davies, R., et al. 2009, J. Inst., submitted, (companion paper)
de Gasperis, G., Balbi, A., Cabella, P., Natoli, P., & Vittorio, N. 2005, A&A, 436, 1159
de Zotti, G., Ricci, R., Mesa, D., et al. 2005, A&A, 431, 893
Draine, B. T. & Lazarian, A. 1998, ApJ, 494, L19+
Dunkley, J., Komatsu, E., Nolta, M. R., et al. 2009, ApJS, 180, 306
Dupac, X. & Tauber, J. 2005, A&A, 430, 363
Efstathiou, G. 2004, MNRAS, 349, 603
Efstathiou, G. & Gratton, S. 2009, ArXiv e-prints 0903.0345
Eriksen, H. K., Hansen, F. K., Banday, A. J., Górski, K. M., & Lilje, P. B. 2004a, ApJ, 605, 14
Eriksen, H. K., Hansen, F. K., Banday, A. J., Górski, K. M., & Lilje, P. B. 2004b, ApJ, 609, 1198
Fermi/LAT Collaboration: W.B. Atwood. 2009, ArXiv e-prints 0902.1089
Frailis, M., Maris, M., Zacchei, A., et al. 2009, J. Inst. submitted, (companion

paper)
Gentili, G., Nesti, R., Peolsi, G., & Natale, V. 2000, Electr. Lett., 36, 486
Gold, B., Bennett, C. L., Hill, R. S., et al. 2009, ApJS, 180, 265
Gorski, K. M. 1994, ApJ, 430, L85
Górski, K. M., Hivon, E., Banday, A. J., et al. 2005, ApJ, 622, 759
Gruppuso, A., De Rosa, A., Cabella, P., et al. 2009, submitted to MNRAS, ArXiv e-prints 0904.0789
Hamimeche, S. & Lewis, A. 2008, Phys. Rev. D, 77, 103013
Hansen, F. K., Banday, A. J., & Górski, K. M. 2004, MNRAS, 354, 641
Haverkorn, M., Carretti, E., McConnell, D., et al. 2007, in Bulletin of the American Astronomical Society, Vol. 38, Bulletin of the American Astronomical Society, 123–+
Herranz, D., López-Caniego, M., Sanz, J. L., & González-Nuevo, J. 2009, MNRAS, 394, 510
Hildebrandt, S. R., Rebolo, R., Rubiño-Martín, J. A., et al. 2007, MNRAS, 382, 594
Hinshaw, G., Banday, A. J., Bennett, C. L., et al. 1996, ApJ, 464, L17+
Holman, R. & Tolley, A. J. 2008, Journal of Cosmology and Astro-Particle Physics, 5, 1
Hooper, D., Finkbeiner, D. P., & Dobler, G. 2007, Phys. Rev. D, 76, 083012
Hooper, D., Zaharijas, G., Finkbeiner, D. P., & Dobler, G. 2008, Phys. Rev. D, 77, 043511
Janssen, M. A. & Gulkis, S. 1992, in NATO ASIC Proc. 359: The Infrared and Submillimetre Sky after COBE, ed. M. Signore & C. Dupraz, 391–408
Jewell, J., Levin, S., & Anderson, C. H. 2004, ApJ, 609, 1
Keck, F. 2008, Planck SOVT1 Test Report, Tech. Rep. PT-PMOC-OPS-RP-6414-OPS-OAP, ESOC Documentation
Keihänen, E., Keskitalo, R., Kurki-Suonio, H., Poutanen, T., & Sirviö, A.-S. 2009, in preparation
Keihänen, E., Kurki-Suonio, H., & Poutanen, T. 2005, MNRAS, 360, 390
Keskitalo, R., Ashdown, M. A. J., Baccigalupi, C., et al. 2009, in preparation
Knox, L. 1995, Phys. Rev. D, 52, 4307
Kogut, A., Fixsen, D. J., Levin, S. M., et al. 2009, ArXiv e-prints 0901.0562
Komatsu, E., Dunkley, J., Nolta, M. R., et al. 2009, ApJS, 180, 330
Kurki-Suonio, H., Keihanen, E., Keskitalo, R., et al. 2009, submitted to A&A, ArXiv e-prints 0904.3623
La Porta, L., Burigana, C., Reich, W., & Reich, P. 2008, A&A, 479, 641
Lamarre, J. M., Puget, J. L., Ade, P. A. R., et al. 2009, A&A, submitted, (companion paper)
Land, K. & Magueijo, J. 2005, Physical Review Letters, 95, 071301
Lazarian, A. & Finkbeiner, D. 2003, New Astronomy Review, 47, 1107
Leach, S. M., Cardoso, J.-F., Baccigalupi, C., et al. 2008, A&A, 491, 597
Leahy, J., Bersanelli, M., D'Arcangelo, O., et al. 2009, A&A, submitted, (companion paper)
Lin, Y.-T., Partridge, B., Pober, J. C., et al. 2009, ApJ, 694, 992
Lineweaver, C. H., Smoot, G. F., Bennett, C. L., et al. 1994, ApJ, 436, 452
Maino, D., Burigana, C., Maltoni, M., et al. 1999, A&AS, 140, 383
Mandolesi, N., Bersanelli, M., Burigana, C., et al. 2000, A&AS, 145, 323
Mandolesi, N., Smoot, G. F., & Bersanelli, M. 1994, in Lecture Notes in Physics, Berlin Springer Verlag, Vol. 429, Present and Future of the Cosmic Microwave Background, ed. J. L. Sanz, E. Martinez-Gonzalez, & L. Cayon, 228–+
Maris, M., Bersanelli, M., Burigana, C., et al. 2006a, Memorie della Società Astronomica Italiana Supplement, 9, 460
Maris, M. & Burigana, C. 2009, ArXiv e-prints 0902.0468
Maris, M., Burigana, C., & Fogliani, S. 2006b, A&A, 452, 685
Massardi, M., López-Caniego, M., González-Nuevo, J., et al. 2009, MNRAS, 392, 733
Mennella, A., Bersanelli, M., Aja, B., et al. 2009, A&A, submitted, (companion paper)
Mennella, A., Bersanelli, M., Burigana, C., et al. 2002, A&A, 384, 736
Miville-Deschênes, M.-A. & Lagache, G. 2005, ApJS, 157, 302
Morgante, G., Lapolla, M., Franceschet, C., et al. 2009a, J. Inst., submitted, (companion paper)
Morgante, G., Pearson, D., Stassi, P., et al. 2009b, J. Inst., submitted, (companion paper)
Natoli, P., de Gasperis, G., Gheller, C., & Vittorio, N. 2001, A&A, 372, 346
Paladini, R., Burigana, C., Davies, R. D., et al. 2003, A&A, 397, 213
Pasian, F., Bersanelli, M., & Mandolesi, N. 2000, Baltic Astronomy, 9, 511
Pasian, F. & Gispert, R. 2000, Astrophysical Letters Communications, 37, 247
Pasian, F. & Sygnet, J.-F. 2002, in Society of Photo-Optical Instrumentation Engineers (SPIE) Conference Series, Vol. 4847, Society of Photo-Optical Instrumentation Engineers (SPIE) Conference Series, ed. J.-L. Starck & F. D. Murtagh, 25–34
Pearson, T. J. & C-BASS collaboration. 2007, in Bulletin of the American Astronomical Society, Vol. 38, Bulletin of the American Astronomical Society, 883–+
Pelkonen, V.-M., Juvela, M., & Padoan, P. 2007, A&A, 461, 551
Perrotta, F. & Maino, D. 2007, Planck LFI - SGS2 End-to-End test report, Tech. Rep. PL-LFI-OAT-RP-010, LFI DPC Documentation
Ponthieu, N., Macías-Pérez, J. F., Tristram, M., et al. 2005, A&A, 444, 327
Poutanen, T., de Gasperis, G., Hivon, E., et al. 2006, A&A, 449, 1311
Reinecke, M., Dolag, K., Hell, R., Bartelmann, M., & Enßlin, T. A. 2006, A&A, 445, 373
Rocha, G., Contaldi, C., Colombo, L., et al. 2009, in preparation
Rubino-Martin, J. A., Rebolo, R., Tucci, M., et al. 2008, ArXiv e-prints 0810.3141
Sandri, M., Villa, F., Bersanelli, M., et al. 2009, A&A, submitted, (companion paper)
Sandri, M., Villa, F., Nesti, R., et al. 2004, A&A, 428, 299
Schwarz, D. J., Starkman, G. D., Huterer, D., & Copi, C. J. 2004, Physical Review Letters, 93, 221301
Smith, K. M., Senatore, L., & Zaldarriaga, M. 2009, ArXiv e-prints 0901.2572
Smith, K. M. & Zaldarriaga, M. 2006, ArXiv e-prints astro-ph/0612571
Smoot, G. F., Bennett, C. L., Kogut, A., et al. 1992, ApJ, 396, L1
Tauber, J., Mandolesi, N., Puget, J.-L., et al. 2009, A&A, submitted, (companion paper), XXX
Tauber, J., Pace, O., & Volonte, S. 1994, ESA Journal, 18, 239
Tegmark, M. 1997, ApJ, 480, L87+
Tegmark, M., de Oliveira-Costa, A., & Hamilton, A. J. 2003, Phys. Rev. D, 68, 123523
Terenzi, L., Bersanelli, M., Battaglia, P., et al. 2009a, J. Inst., submitted, (companion paper)
Terenzi, L., Bersanelli, M., Mennella, A., et al. 2009b, J. Inst., submitted, (companion paper)
The Planck Collaboration. 2006, ArXiv e-prints astro-ph/0604069
Umana, G., Burigana, C., & Trigilio, C. 2006, Memorie della Società Astronomica Italiana Supplement, 9, 279
Valenziano, L., Cuttaia, F., De Rosa, A., et al. 2009, J. Inst., submitted, (companion paper)
Valenziano, L., Villa, F., Mandolesi, N., & Bersanelli, M. 1998, Focal Surface Evaluation for the Planck Telescope, Tech. Rep. 224/1998, TeSRE/CNR - Bologna
Varis, J., Hughes, N., Laaninen, M., et al. 2009, J. Inst., submitted, (companion paper)
Vielva, P., Martínez-González, E., Barreiro, R. B., Sanz, J. L., & Cayón, L. 2004, ApJ, 609, 22
Vielva, P., Wiaux, Y., Martínez-González, E., & Vandergheynst, P. 2007, MNRAS, 381, 932
Villa, F., Burigana, C., & Mandolesi, N. 1998, A Note on the Planck Aplanatic Telescope, Tech. Rep. 221/1998, TeSRE/CNR - Bologna
Villa, F., D'Arcangelo, O., Pecora, M., et al. 2009a, J. Inst. submitted, (companion paper)
Villa, F., Sandri, M., Mandolesi, N., et al. 2002, Experimental Astronomy, 14, 1
Villa, F., Terenzi, L., Sandri, M., et al. 2009b, A&A, submitted, (companion paper)
Wade, L., Bhandari, P., Bowman, J., et al. 2000, Advances in Cryogenic Engineering, 45
Waelkens, A., Jaffe, T., Reinecke, M., Kitaura, F. S., & Enßlin, T. A. 2009, A&A, 495, 697
Wandelt, B. D., Larson, D. L., & Lakshminarayanan, A. 2004, Phys. Rev. D, 70, 083511
Weeks, J. R. 2004, ArXiv e-prints astro-ph/0412231
Wiaux, Y., Vielva, P., Martínez-González, E., & Vandergheynst, P. 2006, Physical Review Letters, 96, 151303
Wright, E. L., Chen, X., Odegard, N., et al. 2009, ApJS, 180, 283
Wright, E. L., Hinshaw, G., & Bennett, C. L. 1996, ApJ, 458, L53+
Yadav, A. P. S., Komatsu, E., & Wandelt, B. D. 2007, ApJ, 664, 680
Zacchei, A., Frailis, M., Maris, M., et al. 2009, J. Inst. submitted, (companion paper)

[1] IASF - BO, INAF, Bologna, Italy
[2] Dipartimento di Fisica, Università degli Studi di Milano, Italy
[3] Osservatorio Astronomico di Padova, INAF, Italy
[4] Dipartimento di Fisica, Università degli Studi di Padova, Italy
[5] Dipartimento di Fisica, Università degli Studi di Roma "Tor Vergata", Italy
[6] INAF – Osservatorio Astronomico di Trieste, Via G.B. Tiepolo 11, I-34131, Trieste, Italy
[7] Dep. Ing. de Comunicaciones (DICOM), Universidad de Cantabria Av. De Los Castros S/N, 39005 Santander, Spain
[8] SISSA/ISAS, Astrophysics Sector, via Beirut 2-4, Sezione di Trieste, I-34014, Trieste, Italy

[9] MPA - Max-Planck-Institut für Astrophysik, Karl-Schwarzschild-Str. 1, 85741 Garching, Germany
[10] Jet Propulsion Laboratory, California Institute of Technology 4800 Oak Grove Drive, Pasadena, CA 91109, USA
[11] ISDC Data Centre for Astrophysics, University of Geneva, ch. d'Ecogia 16, CH-1290 Versoix, Switzerland
[12] Herschel/Planck Project, Scientific Projects Dpt of ESA, Keplerlaan 1, 2200 AG, Noordwijk, The Netherlands
[13] IFP-CNR Milano, Italy
[14] Jodrell Bank Centre for Astrophysics, University of Manchester, M13 9PL, UK
[15] ASI, Agenzia Spaziale Italiana, Roma, Italy
[16] Dipartimento di Fisica, Università di Trieste, Trieste, Italy
[17] Instituto de Fisica de Cantabria, CSIC- Universidad de Cantabria, Avenida de los Castros s/n, 39005 Santander, Spain
[18] Instituto de Astrofisica de Canarias, La Laguna, Tenerife, Spain
[19] University of Helsinki, Department of Physics, P.O. Box 64, FIN-00014 Helsinki, Finland
[20] Metsähovi Radio Observatory, TKK, Helsinki University of Technology, Metsähovintie 114, FIN-02540 Kylmälä, Finland
[21] Physics Department, University California at Santa Barbara, USA
[22] Institute of Theoretical Astrophysics, and Centre of Mathematics for Applications, University of Oslo Norway
[23] ESA/ESAC/RSSD, Villanueva de la Cañada Madrid, Spain
[24] Osservatorio Astronomico di Arcetri, L.go E. Fermi 5, Firenze, Italy
[25] Haverford College, Haverford PA, USA
[26] Research and Scientific Support Department of ESA, ESTEC, Noordwijk, The Netherlands
[27] Institute for Space Science, Bucharest-Magurele, Romania
[28] LBNL, Berkeley, USA
[29] University of British Columbia, Vancouver, British Columbia, Canada
[30] Oxford Univ., Nuclear and Astrophysics Laboratory - Astrophysics, Oxford, UK
[31] Physics Department, University of California at Berkeley, Ewha University, and Univ. d'Paris Diderot
[32] MilliLab, VTT Technical Research Centre of Finland, Espoo, Finland
[33] Helsinki Institute of Physics, P.O. Box 64, FIN-00014 Helsinki, Finland
[34] OABO, INAF, Bologna, Italy
[35] INFN, Sezione di Trieste, I-34014, Trieste, Italy
[36] INFN, Sezione di Tor Vergata, I-00133, Roma, Italy
[37] University of California, Berkeley Space Sciences Lab 7 Gauss Way Berkeley, CA, USA
[38] Computational Research Division, Lawrence Berkeley National Laboratory, Berkeley, CA, USA
[39] CESR, Centre d'Etude Spatiale des Rayonnements, 9, av du Colonel Roche, BP 44346 31028 Toulouse Cedex 4, FRANCE
[40] ESA - ESAC, Villafranca del Castillo, Apdo. 50727, 28080 Madrid, Spain
[41] Warsaw University Observatory, Aleje Ujazdowskie 4, 00-478 Warszawa, Poland
[42] Astrophysics Group, Cavendish Laboratory, J.J. Thomson Avenue, CB3 0HE, Cambridge, United Kingdom
[43] Department of Physics, University of Miami, Coral Gables, FL, USA
[44] ASI Science Data Center, c/o ESRIN, via G. Galilei snc, I-00044 Frascati, Italy
[45] Dipartimento di Fisica, Universita di Roma La Sapienza, p.le A. Moro 2, I-00185 Roma, Italy